

SOOT DEPOSITION FROM ETHYLENE/AIR FLAMES AND THE ROLE OF AROMATIC INTERMEDIATES. Joanne M. Smedley and Alan Williams. Department of Fuel and Energy, Leeds University, Leeds, LS2 9JT, UK.

ABSTRACT

The formation of soot is of interest as a pollutant but also because it forms deposits in combustion chambers. In this work a McKenna flat flame, water-cooled, premixed burner was used to study soot deposition from two rich ethylene/air flames ($\phi = 2.52$, $\phi = 2.76$). Rates of soot deposition for both cooled copper and uncooled stainless steel surfaces were investigated. Soot samples from these experiments were analysed for PAH by solvent extraction. Temperature profiles were taken using Pt/Pt 13% Rh thermocouples. A quartz microprobe sampling system was used in conjunction with a gas chromatograph to determine the concentration profiles of aromatic and polyaromatic species in the deposition region. Experimental results indicate that soot deposition occurs by a thermophoretic mechanism when cooled surfaces are used and that soot deposition rates increase as samples are taken further in the flame zone. If uncooled surfaces are used then direct surface deposition takes place. The chemical mechanisms involved are discussed.

INTRODUCTION

The formation and deposition of soot in any combustion system is undesirable. Soot deposits can have adverse effects on heat transfer characteristics or combustion behaviour which can cause performance or failure problems in a range of systems from rocket engines to diesels. The emission of soot particles from combustion chambers into the atmosphere is also of environmental concern due to the fact that soot particles can contain significant concentrations of PAH. There is thus a need to accurately predict under what conditions soot formation will occur and to quantify the amount of soot deposited in any part of a combustion system.

Over recent years more progress has been made in understanding the chemical route of soot formation but work in this area is difficult due to the complex interaction of aromatic species in sooting flames (1-5). Harris et al (1) have attempted to model single ring aromatic species but have only succeeded in modelling benzene because of the complexity of the subsequent growth steps. They encountered the problem that most of the rate constant data must be estimated since absolute values are not available. Minor species such as C_2H_2 have been accurately modelled by Miller et al (2) and Harris et al (3) as more reliable data are available for these species. Even though these models exist, many gaps remain in the mechanism of the subsequent steps leading to soot formation. Whilst acetylene is recognised as a major growth species there is uncertainty about the level of participation of the PAH species. Soot deposition onto a cooled surface has been recently investigated by Makel and Kennedy (4) using a laser diagnostic technique to measure soot deposit thickness and free stream soot concentrations. A numerical model to make predictions of soot deposition rate was also developed by them.

EXPERIMENTAL METHODS

Two rich ethylene/air flames ($\phi = 2.52$ and $\phi = 2.76$) were studied using a flat flame, water-cooled, premixed burner (McKenna Industries). The gas flows in litres/minute for the $\phi = 2.52$ flame were $O_2 = 2.22$, $N_2 = 8.36$, $C_2H_4 = 1.79$ and the flows for the $\phi = 2.76$ flame were $O_2 = 2.36$, $N_2 = 8.90$, $C_2H_4 = 2.09$. To investigate soot deposition rates an uncooled stainless steel plate and a cooled copper plate were used to support stainless steel and copper sample squares respectively within the flame. The sample plate dimensions were approximately

10 mm x 10 mm x 2 mm. Four flame heights were of interest, these were 5, 10, 15 and 20 mm above the burner surface. At each height weighed sample plates were inserted into the flame for intervals of 15 seconds (from 15 to 75 seconds) and were reweighed after to give the weight of soot produced.

The PAH content of some of the soot collected was determined using a solvent extraction process. Deposited soot from the metal plate and free steam soot which was collected on a Whatman glass microfilter GF/C paper from both flames was analysed using a pyrolysis chromatography. A Perkin Elmer 8320 gas chromatograph fitted with a Quadrax 007' series fused silica capillary column was coupled with a CDS Pyroprobe to desorb hydrocarbons from the soot. Approximately 2.5 mg of soot is heated at a rate of 0.1°C per millisecond up to 600°C. A quartz microprobe with a 6 mm outside diameter similar to that used by Harris et al (3) was used to obtain gas samples at various heights above the burner surface and a syringe method was used to transfer samples into a gas chromatograph (Perkin Elmer 8700 gas chromatograph fitted with a J & W megabore GS-Q column).

RESULTS AND DISCUSSION

Soot Deposition

Figures 1 and 2 give typical experimental data for the rate of soot deposition for the uncooled and cooled plates. In these each line represents different sampling heights above the burner. As expected the deposition rate of soot increases on an uncooled stainless steel plate as the plate is moved vertically away from the burner surface. However the deposition rate of soot at 20 mm above the burner surface is less than the deposition rate at 15 mm above the burner surface when the water cooled copper plate is used. This was found to occur in both flames ($\phi = 2.52$ and $\phi = 2.76$). It has been observed that the ultimate soot load on sample squares is approximately 0.7 mg regardless which plate is used. For the uncooled plate a 0.7 mg soot load occurs at 20 mm but when using the water cooled plate a soot loading of 0.7 mg is achieved at 15 mm when both had 75 seconds exposure in the flame. It is thought that above 0.7 mg the soot load is too great and the soot breaks off and is dispersed back into the flame. This is why a reduced soot deposition rate is seen for the 20 mm height samples when using the water-cooled plate. In general, for both plates the soot deposition rates are greater for the $\phi = 2.76$ flame at all heights than for the $\phi = 2.52$ flame. The exception for the metal plate is at 20 mm. Similar rates are experienced for both flames at this height and this again suggests that there is a limit to the amount of soot that can be deposited under these conditions.

When comparing the results from the uncooled plate and water cooled plate for $\phi = 2.52$ flame it can be seen the soot deposition rate at 10 mm above the burner surface for the uncooled plate is much less than the soot deposition at the same height for the cooled plate. For example, at 75 seconds a soot load of under 0.1 mg is recorded for the uncooled plate. Whereas on the water cooled plate a soot load of approximately 0.4 mg is recorded at 75 seconds. The same is noticed at 15 mm above the burner surface at 75 seconds. The uncooled plate has a soot load of 0.4 mg while the cooled plate has a soot load of 0.55 mg. This is consistent with the thermophoretic transport of soot particles. From the results it also seems that thermophoresis is more prominent at lower regions in the flame. This may be because the soot particles are smaller earlier in the flame and as they become larger later thermophoresis has less influence on the movement of the soot particles. Makei and Kennedy (4) assumed that thermophoresis was the primary transport process for soot particles (-10 - 100 nm in diameter) although no allowance was made for variation in particle size. He also experienced the process of resuspension when the soot load increases to a certain limit. This was incorporated into his model to try and determine the final soot loading.

The soot mass flux to the surface can be expressed (4) as

$$J''_{\text{tot}} = \rho_s V_d \phi_{s,z} \quad (1)$$

where ρ_s is the particle density (1900 kg/m^3), $\phi_{s,z}$ is the soot volume fraction at the edge of the diffusion sublayer and the deposit velocity, V_d , is equal to the thermophoretic drift velocity, V_t , given by

$$V_t = -0.55 \nu d (\ln T)/dy \quad (2)$$

where ν is the viscosity and which is largely determined by the temperature gradient.

Experimental deposition rates were found to be $1 \times 10^{-2} \text{ mg/cm}^2 \text{ s}$ at 15 mm above the burner using the water-cooled plate and $0.75 \times 10^{-2} \text{ mg/cm}^2 \text{ s}$ using the uncooled metal plate. This is consistent with Makel and Kennedy's experimental data although they used a water-cooled cylinder to collect their samples. The calculated deposition value for our experiments using their theory is $1.2 \times 10^{-2} \text{ mg/cm}^2 \text{ s}$ for the water-cooled plate and $0.6 \times 10^{-2} \text{ mg/cm}^2 \text{ s}$ for the uncooled plates. The agreement is excellent.

PAH Content of the Soots

Deposited soot samples at 20 mm above the burner were collected from both flames after 75 seconds exposure within the flame. These soot samples were analysed in the Pyroprobe apparatus. Some results from this experiment are shown in Figures 3 and 4. Most of the peaks in the chromatograph were identified using a standard PAH mixture or by using retention indices (5-7). The major peaks are identified in Fig. 3. The gas chromatograph results for both the flames studied were very similar. Generally each PAH component was found in greater quantities in the richer $\phi = 2.76$ flame. The $\phi = 2.52$ flame contained much more volatile material which is expelled from the soot very early and is the first peak. The $\phi = 2.52$ also contained more amounts of the larger components such as benzopyrenes and other 5-ring compounds which occur in the latter part of the chromatogram. Larger ring compounds also exist in both flames.

Free stream soot samples were collected on to Whatman glass microfibre filters were also analysed using the Pyroprobe system. Results from the $\phi = 2.76$ flame are shown in Figure 4a. The collecting conditions for the free stream soot are identical to those quoted above for the deposited soot samples. When comparing the results from the free stream soot and the results for the soot deposited on the uncooled plate (Figure 4b) it is noted that the free stream soot always contains greater amounts of the 2 and 3 ring compounds such as acenaphthylene and the deposited soot always contains larger amounts of the 4 and 5 ring compounds like pyrene and also 6 and 7-ring compounds. This may be because the filter paper collection is at a lower temperature which favours the absorption of the smaller volatile gas phase material. If this is not the case there are important implications to the ability of soot to have varying compositions depending on whether it is in the gas phase or deposited on a surface.

Soot Formation Steps

Figure 5 shows the gas composition profiles obtained using the quartz probe sampling system. The reaction zone (based on O_2 decay) is quite extended. Figure 6 shows profiles of some aromatic species and their precursors. The results show that as combustion takes place C_2H_4 and O_2 are depleted. In Fig. 6 it can be seen that C_2H_2 peaks at about 5 mm above the burner after which it levels off to a fairly constant value between 10 and 20 mm. C_6H_6 rises gradually at about 6 mm and begins to fall at 12 mm. Initially there was more C_6H_6 in the $\phi = 2.52$ flame but at 20 mm there was more in the $\phi = 2.76$ flame. Laser beam

attenuation studies at 670 nm indicated that soot formation began at 6 mm above the burner. From the results it can be seen that as C_2H_2 is consumed C_6H_6 is produced as well as soot; this is consistent with the fact that C_2H_2 is involved in C_6H_6 formation and it is generally considered that C_2H_2 is an important precursor to soot formation. C_2H_2 and C_6H_6 fall as soot is formed and other larger hydrocarbons are produced in the flame. In Fig. 5 both CO and H_2 increase gradually as the probe is moved away from the burner surface. It was found that H_2 was in greater concentration in the $\phi = 2.52$ flame and CO was in a higher concentration initially. O_2 was only found in small amounts in the $\phi = 2.52$ flame. These increase as combustion takes place and are products of oxidation reactions. These trends were seen by Harris (3) et al but they only probed to about 3 mm above burner so they did not observe the fall in C_2H_2 and C_6H_6 in the later part of the flame. Miller (2) et al however undertook experiments up to 22.5 mm and also found similar profiles for CO, O_2 and H_2 .

The mechanism of soot formation from an ethylene flame involves the formation of acetylene and its polymerisation to single and then multi-ring species. The subsequent growth of the initial soot particles involves surface growth involving acetylene and polyaromatic species the relative extent of them being subject to different interpretation (eg. 5, 8 and 9). In the free stream soot samples taken here the product involves soot particles, surface adsorbed PAH and gas phase PAH. However the deposited samples can only contain PAH associated with the soot particles as adsorbed or growth species. The deposited samples are significantly different to the free stream soot in that the dominant PAH species are the 4+ ring species and smaller species are present in lower concentrations.

The suggestion must be implicit in these findings that the acetylene grows on the soot surface generating multi-ring compounds there which ultimately become part of the soot particle. During pyrolysis gc these compounds are desorbed as shown in the experimental results.

CONCLUSIONS

1. The deposition rate of soot increases with height above the burner surface (up to 20 mm) and sampling time (up to 75 seconds). More soot is deposited as ϕ is increased, but there seems to be a limit in the amount of soot that can be deposited regardless of the method of deposition because of soot break off at relatively low loadings.
2. There is evidence that thermophoresis is involved in soot deposition on to a cooled plate and that it is more dominant earlier in the flame when soot particles are smaller. The measured rates are consistent with the values calculated using the model proposed by Makei and Kennedy.
3. Soot samples from the uncooled metal plate contain large aromatic compounds with 4 and 5 and larger rings. The $\phi = 2.52$ had a higher concentration of some of these compounds.
4. Free stream soot samples contain a higher concentration of 2 and 3 ring aromatics than deposited soot. Higher concentrations of 4 and 5 ring aromatics were found in the deposited soot for the same conditions. This implies that these compounds are implicated in the soot growth mechanism.

ACKNOWLEDGEMENTS

One of us (JMS) wishes to thank the Esso Petroleum Company for an SERC CASE Studentship. We also wish to acknowledge assistance from Dr. K.D. Bartle, Mr. J.M. Taylor, Miss A.L. Thomas and Mrs. Mutshimwong.

REFERENCES

1. Harris, S.J., Weiner, A.M. and Blint, R.J. *Combustion and Flame* 72, 91-109 (1988).
2. Miller, J.A., Volponi, J.V., Durant, Jr. J.L., Goldsmith, J.E.M., Fisk, G.A. and Kee, R.J. *Twenty-third Symposium (International) on Combustion*, The Combustion Institute (1990).
3. Harris, S.J., Weiner, A.M. and Blint, R.J. *Twenty-first Symposium (International) on Combustion*, The Combustion Institute, pp 1033-1045 (1986).
4. Makel, D.B and Kennedy, I.M. *Twenty-third Symposium (International) on Combustion*, The Combustion Institute (1990).
5. Lam, F.W., Howard, J.B. and Longwell, J.P. *Twenty-second Symposium (International) on Combustion*, The Combustion Institute, pp 323-331 (1988).
6. Bartle, K.D. *Handbook of Polycyclic Aromatic Hydrocarbons*, Vol. 2, p 193 (edit. Bjorscth and Randahl) (1985).
7. Rostad, C.E. and Pereira, W.E. *J. of High Resolution Chromatography and Chromatography Communicators*, p 328 (1986).
8. Frenklach, M., Clary, D.W., Gardiner, Jr. W.C. and Stein, S.E. *Twentieth Symposium (International) on Combustion*, The Combustion Institute, pp 887-896 (1984).
9. Harris, S.J. and Weiner, A.M. *Twenty-second Symposium (International) on Combustion*, The Combustion Institute, pp 333-339 (1988).

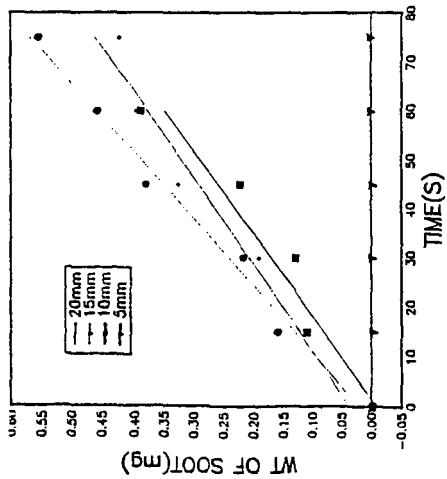


Fig. 1. Plot of soot deposition against time for water-cooled plate, $\phi = 2.52$.

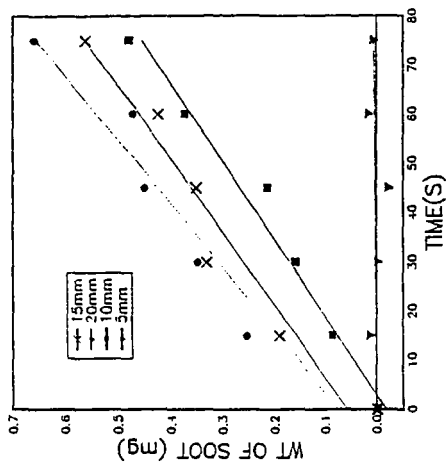


Fig. 2. Plot of soot deposition against time for uncooled metal plate, $\phi = 2.76$.

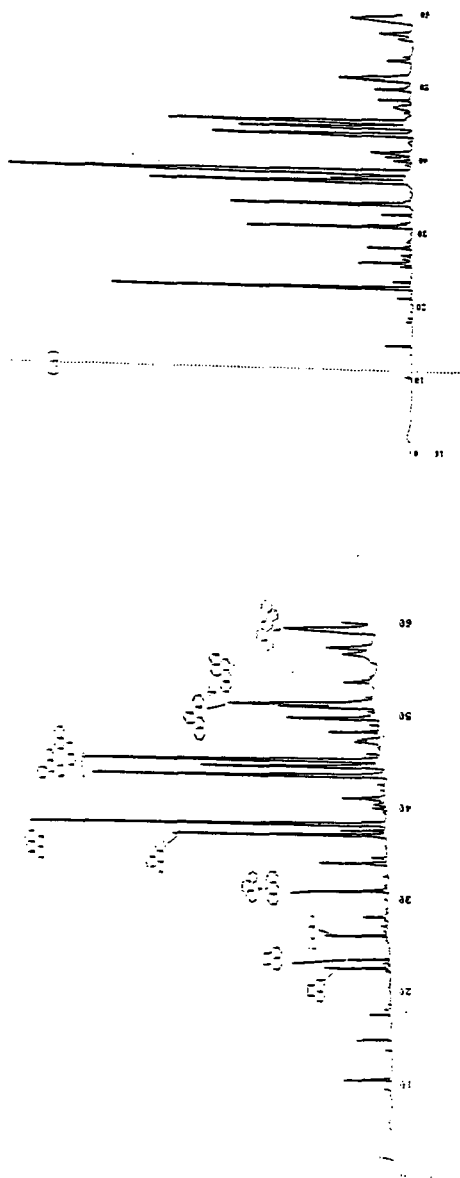


Fig. 3. Gas chromatogram with major peaks labelled sample for uncoated metal plate, $\phi = 2.76$.

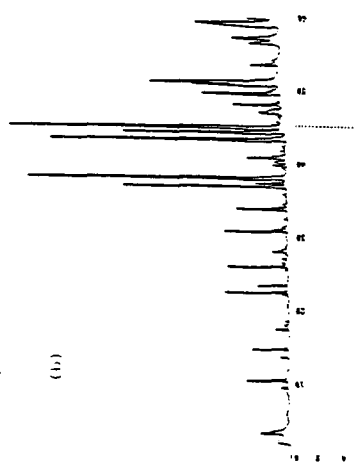


Fig. 4 (a) Gas chromatogram of free stream soot at 15 mm above burner, $\phi = 2.76$.
 (b) Gas chromatogram of deposited soot at same conditions.

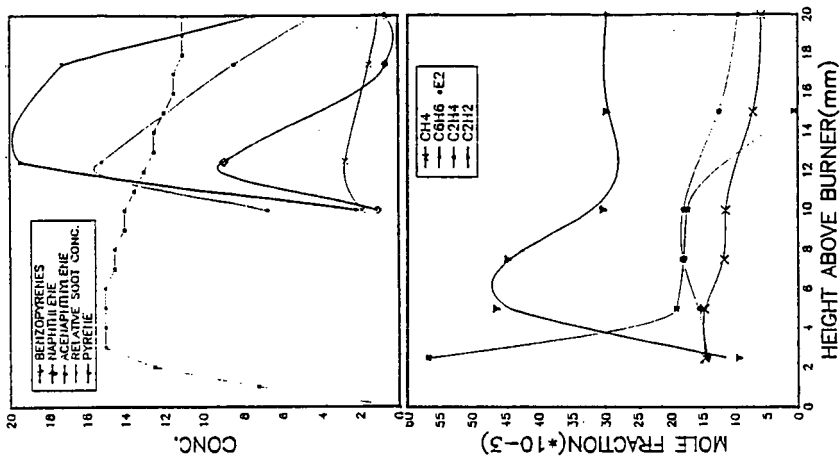


Fig. 5. Small molecule species profiles for $\phi = 2.76$ flame (mol fraction).

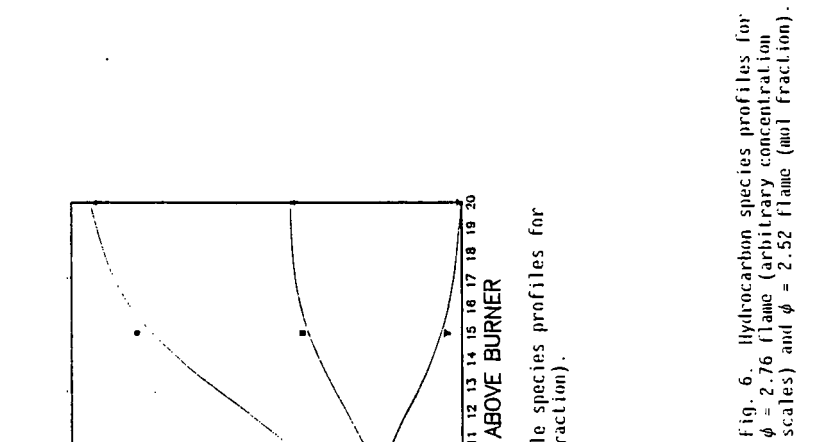


Fig. 6. Hydrocarbon species profiles for $\phi = 2.76$ flame (arbitrary concentration scales) and $\phi = 2.52$ flame (mol fraction).

AROMATICS GROWTH BEYOND THE FIRST RING AND THE NUCLEATION OF SOOT PARTICLES

Michael Frenklach and Hai Wang
 Fuel Science Program
 Department of Materials Science and Engineering
 The Pennsylvania State University
 University Park, PA 16802

Keywords: soot formation, reaction mechanism and chemical kinetics of, particle dynamics of

INTRODUCTION

In this manuscript, we discuss the the reaction mechanism responsible for the formation and growth of polycyclic aromatic hydrocarbons (PAHs) and subsequent nucleation and growth of soot particles in combustion of hydrocarbon fuels. The discussion is based on the results of a detailed chemical kinetic study,¹ and we refer the reader to this reference for the computational details. Here, we focus on the principal reaction pathways and mechanistic features identified in the analysis.

OVERALL PROCESS

The overall model of soot formation can be thought of as consisting of four major processes: *initial PAH formation*, which includes the formation of the first aromatic ring in an aliphatic system; *planar PAH growth*, comprised of replicating-type growth; *particle nucleation*, consisting of coalescence of PAHs into three-dimensional clusters; and *particle growth* by coagulation and surface reactions of the forming clusters and particles. Our primary attention in this discussion is on the last three processes, although some comments are pertinent concerning the formation of the first aromatic ring.

Formation of the First Aromatic Ring

The formation of the first aromatic ring in flames of nonaromatic fuels begins usually with vinyl addition to acetylene. At high temperatures, it forms vinylacetylene followed by acetylene addition to *n*-C₄H₃ radical formed by the H-abstraction from the vinylacetylene (Fig. 1). At low temperatures, the addition of acetylene to vinyl results in *n*-C₄H₅, which upon addition of acetylene produces benzene. Benzene and phenyl are converted to one another by the H-abstraction reaction and its reverse.

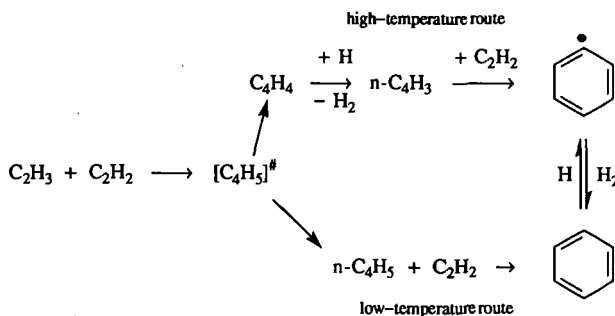


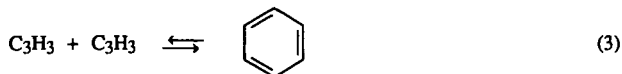
Figure 1. Formation of the first aromatic ring

In a recent review article on chemical kinetics and combustion modeling, Miller, Kee and Westbrook² suggested that the above cyclization reactions cannot be responsible for the formation of the first aromatic ring because the concentrations of *n*-C₄H₃ and *n*-C₄H₅ radicals should be low since the reactions



deplete the concentrations of the *n*-isomers required for the cyclizations. Reactions (1) and (2) were not included in our model. Our computational results indicated that the *n*- and *i*-isomers are already equilibrated by several other reactions in the system. Nonetheless, to test the Miller *et al.*'s suggestion, we performed additional simulations of the three laminar premixed flames we analyzed previously.^{1,3} The reactions (1) and (2) were now included in the simulations assuming rate coefficients $1 \times 10^{14} \text{ mol cm}^{-3} \text{ s}^{-1}$ for the exothermic directions. The results of these simulations for all the three flames tested in Refs. 3 indicated that the inclusion of reactions (1) and (2) — even with upper-limit rate coefficient values — does not make a difference on the computed profile of benzene.

As an alternative, Miller *et al.*² suggested that benzene is formed by combination of propargyl radicals producing benzene or phenyl. A similar proposal was made by Stein *et al.*⁴ Figures 2 and 3 show the results of flame simulations with reaction



included with the rate coefficient of $5 \times 10^{12} \text{ mol cm}^{-3} \text{ s}^{-1}$ suggested by Stein *et al.*⁴ Analysis of these results indicate that the inclusion of cyclization channel (3) does not *always* increase the production rate of benzene, as clearly shown in Fig. 2 for the flame conditions of Harris and co-workers.⁵ For the conditions of the Westmoreland's flame,⁶ the inclusion of reaction (3) significantly overpredicts the amount of benzene determined experimentally (Fig. 3). This is clearly a challenging issue, as the reaction chemistry of C₃H_x species is not well known.

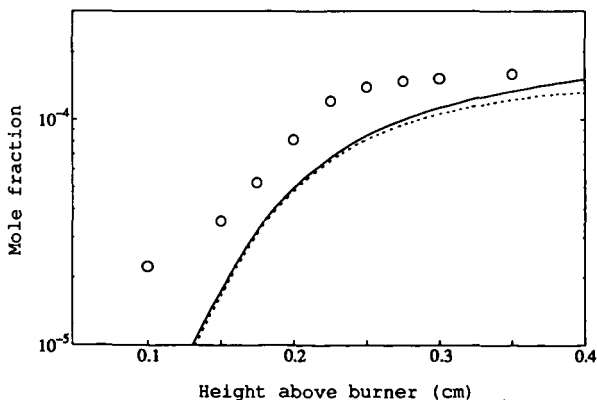


Figure 2. Benzene mole fraction: circles — experimental data,⁵ solid line — computed with the mechanism used in Refs. 1 and 3, dotted line — computed with reaction (3) included

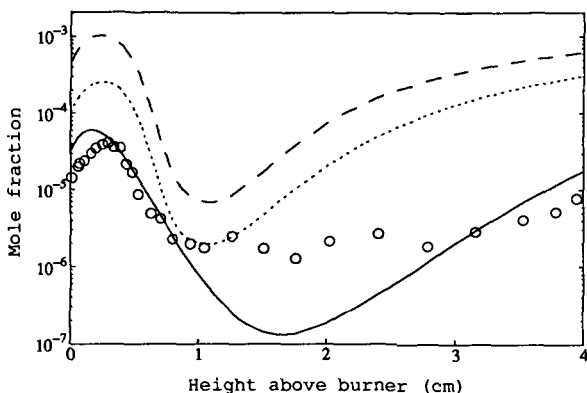


Figure 3. Benzene mole fraction: circles — experimental data;⁶ solid line — computed with the mechanism used in Refs. 1 and 3; dashed and dotted lines — computed with reaction (3) included, dotted line represents the result computed with the mechanism tuned to fit the experimental C_3H_3 profile

Growth of the Aromatic Rings

Once formed, aromatic rings grow by a sequential two-step process: H-abstraction which activates the aromatic molecules, and acetylene addition which propagates molecular growth and cyclization of PAHs (Fig. 4).

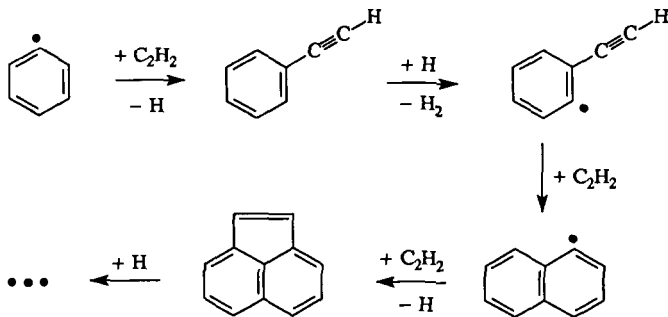


Figure 4. H-abstraction- C_2H_2 -addition reaction pathway of PAH growth

Starting with an aromatic fuel, a "direct" condensation of intact aromatic rings becomes important. For example, in the case of high-temperature pyrolysis of benzene the reactions shown in Fig. 5 were found to dominate the initial stages of PAH growth.⁷

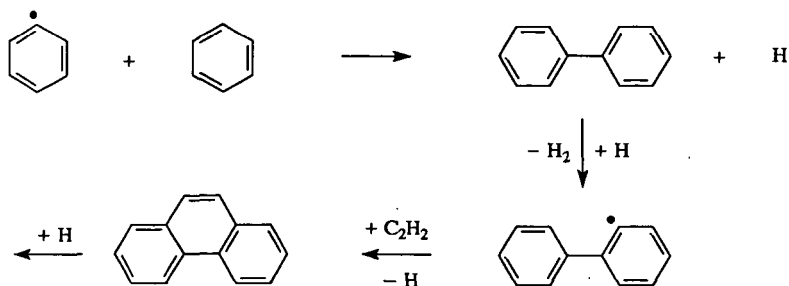
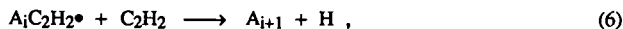


Figure 5. PAH growth initiated by aromatics "condensation"

However, as the reaction progresses, the initial benzene molecules decompose, primarily forming acetylene. As the concentration of acetylene approaches that of benzene, which occurs shortly after the initial period, the PAH growth switches to the acetylene-addition mechanism discussed above for nonaromatic fuels. In other words, the reaction system *relaxes* to the acetylene-addition pathway. The relaxation is faster in oxidation⁸ as compared to pyrolysis and in mixtures of hydrocarbons⁹ as compared to individual fuels.

Some of the acetylene addition reactions in the PAH growth sequence form particularly stable aromatic molecules, like pyrene, coronene, etc. The change of the free energy in these reactions is so large that the reactions become practically irreversible. This, in turn, has an effect of "pulling" the reaction sequence forward, towards formation of larger PAH molecules. Other acetylene addition steps are highly reversible, i.e., the rate of the forward reaction is nearly balanced by the rate of the reverse reaction. These steps with tightly balanced reaction fluxes create a thermodynamic barrier to PAH growth. It is this thermodynamic "resistance" which is responsible for the appearance of most stable, condensed aromatic structures, as opposite to open shell carbon clusters leading to fullerenes.¹⁰ For instance, due to small differences in reaction enthalpies, the reaction flux from phenanthrene to benzo[ghi]perylene shown on the left of Fig. 6 was computed¹¹ to be faster by an order of magnitude than the one on the right hand side of Fig. 6.

The main kinetic features of PAH growth after a certain PAH size, i_0 , can be schematically represented by the following set of reactions¹²



where A_i denotes an aromatic molecule containing i fused aromatic rings ($i = i_0, i_0+1, \dots, \infty$), A_i^\bullet is an aromatic radical formed by the abstraction of an H atom from A_i , and $A_iC_2H_2^\bullet$ is a radical formed by the addition of C_2H_2 to A_i^\bullet . It is assumed that reactions (5) and (6) are reversible and reaction step (6) is irreversible. The rate of PAH mass accumulation is proportional to

$$\text{Rate} = \frac{K_4 \frac{[H]}{[H_2]}}{\frac{1}{K_5 k_6 [C_2H_2]^2} + \frac{1}{k_5 [C_2H_2]} + \frac{1}{k_{-4} [H_2]}} \int r_0 dt, \quad (7)$$

where t is the reaction time, r_0 is the rate of irreversible formation of A_{i0} by initiation reactions, k_j is the rate coefficient of the j th reaction, and $K_j = k_j/k_{-j}$ is the equilibrium constant of the j th reaction.

In this equation, term $\int r_0 dt$ represents the contribution of the initiation reactions, i.e., those leading to the formation of first few PAHs. Term $K_4 \frac{[H]}{[H_2]}$ accounts for the "equilibrium position" or, in more rigorous terms, reaction affinity of reaction (1); it represents the superequilibrium of H atoms — the first kinetic factor responsible for PAH growth. Term $k_6[C_2H_2]$ is the effective rate constant of the irreversible addition of acetylene, reaction (6), forming particular stable PAH molecules — the second kinetic factor responsible for PAH growth. Terms $k_5[C_2H_2]$ and $K_5[C_2H_2]$ specify kinetic and thermodynamic factors, respectively, of the reversible addition of acetylene, reaction (5); the latter expresses the thermodynamic resistance to PAH growth. And finally, term $k_{-4}[H_2]$ accounts for the effective rate constant of the H-abstraction, reaction (4); to illustrate it, consider the limit of $k_{-4}[H_2] \rightarrow 0$ under which condition the ratio in Eq. (7) reduces to $k_4[H]$. At high pressures, reaction



should contribute to the overall balance of the A_i^\bullet radical, and at a high concentration of hydrogen atoms, such that $k_8[H] \gg k_{-4}[H_2]$, we obtain an interesting limit of the PAH growth rate being independent of the H concentration.

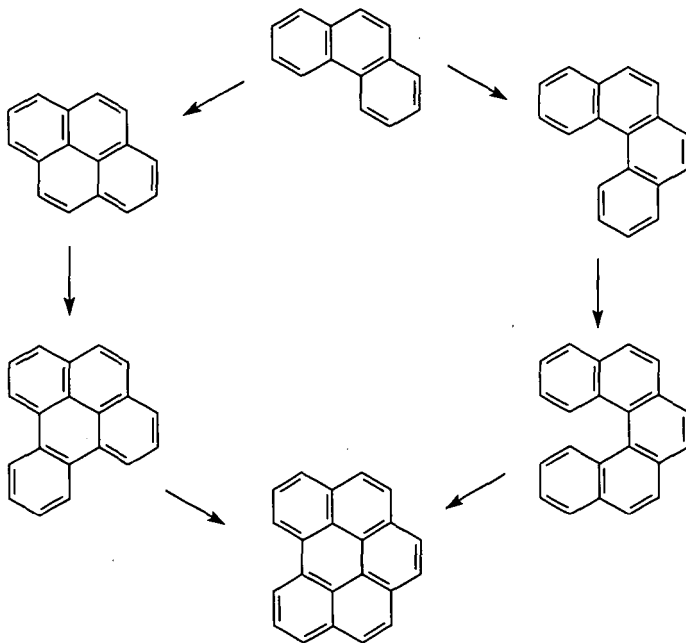


Figure 6. Comparison of two pathways of PAH growth.

An additional kinetic factor, $k_9[\text{O}_2]$, where k_9 is the rate coefficient of oxidation reaction

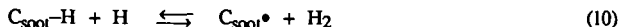


is introduced in oxidative environments. Although many oxidative reaction channels are possible, it appeared, as a result of our kinetic analysis of shock-tube oxidation⁸ and flame¹³ environments, that PAH removal by oxidation occurs predominantly via molecular oxygen attack on aromatic radicals. Also, due to similar reactions of O_2 with C_2H_3 and C_4H_3 radicals (and of OH with C_2H_2 , *etc.*), the concentrations of these critical intermediates are decreased, which in turn reduces the formation rate of the first aromatic ring. At the same time, the presence of O_2 in the mixture has a promoting effect on aromatics formation because of the accelerated chain branching leading to enhanced fuel pyrolysis and thus increased production of critical intermediates and hydrogen atoms. The balance of all of these factors determines the net effect of oxygen addition.

Nucleation and Growth of Soot Particles

We have developed a detailed kinetic model of soot particle formation and growth in the following manner. The formed PAH species were allowed to *coagulate*, that is, all the A_i 's ($i = 4, 5, \dots, \infty$) collide with each other forming dimers; the dimers, in turn, collide with A_i forming trimers or with other dimers forming tetramers; and so on. The coalescence reactions were treated as irreversible having sticking coefficients of unity. As the focus of this work is on very young, small particles, it was assumed that the coagulation dynamics is in the free-molecular regime.

Beginning with the dimers, the forming clusters were assumed to be "solid phase" and allowed to add and lose mass by surface reactions



where $\text{C}_{\text{soot}}\text{-H}$ represents an arm-chair site on the soot particle surface and $\text{C}_{\text{soot}}^\bullet$ the corresponding radical. This mechanism is adopted based on the postulate^{1,14} that the H-abstraction/ C_2H_2 -addition reaction sequence above is responsible for high-temperature growth of all forms of carbonaceous materials. Following this postulate, the rate coefficients of the heterogeneous reactions (10)–(15) were estimated based on analogous gas-phase reactions of one-ring aromatics, benzene and phenyl. In doing so, it was assumed that collision efficiencies on a per-site basis are the same for both gas-phase and gas-solid reactions. The particle dynamics — the evolution of soot particles undergoing simultaneous nucleation, coagulation and surface reactions described above — was modeled by a method of moments which does not require the assumption of a particle size distribution function.

The model predictions were found¹ in relatively close agreement with experiment for such properties as soot particle number density, specific surface area, average soot particle diameter, and laser-light scattering moments for the initial, particle inception part of several simulated laminar premixed flames. The reliability of the model was further supported by the facts that the computed net surface growth rate is in close agreement with that determined by Harris and Weiner¹⁵ and that the predicted rate of soot oxidation by O_2 agrees well with the expression of Nagle and Strickland-Constable.¹⁶

Some major results of this modeling study¹ are summarized below:

- (i) The computed rate of nucleation is balanced by the rate of coagulation throughout the particle inception zone, however, the nucleation rate decays more slowly with flame height than is usually deduced from experiment;
- (ii) Particle inception is primarily determined by PAH coagulation, initiated and controlled by PAH coalescence into dimers. For instance, excluding all surface processes results in a substantial decrease of the particle mass but does not really change the order of magnitude of the particle size. In other words, the particle size is essentially determined by coagulation;
- (iii) While the average soot particle is computed to contain 10^3 – 10^5 carbon atoms, the corresponding average PAH size is only 20 to 50 carbon atoms. This indicates that the crystallites comprising incipient soot particles should be on the order of 7 to 12 Å, in agreement with experiment¹⁷ and against the proposal that soot is formed via spheroidal, polyhedral carbon clusters;
- (iv) The oxidation by OH and O₂ is quite insignificant in the post-flame zone;
- (v) The surface growth of soot mass is primarily determined by two processes: acetylene addition via the H-abstraction/C₂H₂-addition reaction sequence, and PAH condensation on the particle surface. The relative contribution of each of these processes appears to change with experimental conditions. Thus, while the acetylene addition dominates surface growth in an atmospheric ethylene flame of Harris *et al.*,⁵ PAH condensation prevails in a low-pressure acetylene flame of Bockhorn and co-workers.¹⁸ The main contribution of the PAH condensation occurs at the early stages of PAH coagulation;
- (vi) The model predicts the classical structure of soot particles: a less dense particle core, composed of randomly oriented PAH oligomers, and a more dense concentrically-arranged particle shell;
- (vii) Surface processes can be understood in terms of elementary chemical reactions of surface active sites. The number density of these sites is determined by the chemical environment.

ACKNOWLEDGEMENTS

The computations were performed using the facilities of the Pennsylvania State University Center for Academic Computing. Research was sponsored by the Air Force Office of Scientific Research, Air Force Systems Command, USAF, under grant No 88-0072. The US Government is authorized to reproduce and distribute reprints for Governmental purposes notwithstanding any copyright notation thereon.

REFERENCES

1. Frenklach, M. and Wang, H., "Detailed Modeling of Soot Particle Formation and Growth," *Twenty-Third Symposium (International) on Combustion*, in press.
2. Miller, J. A., Kee, R. J. and Westbrook, C. K., *Annu. Rev. Phys. Chem.* 41, 345 (1990).
3. Wang, H. and Frenklach, M., "Modeling of PAH Profiles in Premixed Flames," Fall Technical Meeting of the Eastern States Section of the Combustion Institute, Albany, New York, October 1989.
4. Stein, S. E., Walker, J. A., Suryan, M. M., and Fahr, A., "A New Path to Benzene in Flames," *Twenty-Third Symposium (International) on Combustion*, in press.

5. Harris, S. J., Weiner, A. M., Blint, R. J., and Goldsmith, J. E. M., *Twenty-First Symposium (International) on Combustion*, The Combustion Institute, Pittsburgh, 1988, p.1033; Harris, S.J., Weiner, A.M., and Blint, R.J., *Combust. Flame* **72**, 91 (1988).
6. Westmoreland, P. R., "Experimental and Theoretical Analysis of the Oxidation and Growth Chemistry in a Fuel-Rich Acetylene Flame," Ph.D. thesis, MIT, 1986.
7. Frenklach, M., Clary, D. W., Gardiner, W. C., Jr., and Stein, S. E., *Twenty-First Symposium (International) on Combustion*, The Combustion Institute, Pittsburgh, 1988, p. 1067.
8. Frenklach, M., Clary, D. W., Yuan, T., Gardiner, W. C., Jr., and Stein, S. E., *Combust. Sci. Technol.* **50**, 79 (1986).
9. Frenklach, M., Yuan, T., and Ramachandra, M. K., *Energy & Fuels* **2**, 462 (1988).
10. Frenklach, M. and Ebert, L.B., *J. Phys. Chem.* **92**, 561 (1988).
11. Frenklach, M., Clary, D.W., Gardiner, W.C., Jr., and Stein, S.E., *Twentieth Symposium (International) on Combustion*, The Combustion Institute, 1985, p. 887.
12. Frenklach, M., *Twenty-Second Symposium (International) on Combustion*, The Combustion Institute, Pittsburgh, 1989, p. 1075.
13. Frenklach, M. and Warnatz, J., *Combust. Sci. Technol.* **51**, 265 (1987).
14. Frenklach, M., "A Unifying Picture of Gas-Phase Formation and Growth of PAH, Soot, Diamond and Graphite," in *Carbon in the Galaxy: Studies from Earth and Space*, J. Tarter, S. Chang, and D. J. DeFrees, Eds., NASA CP 3061, 1990, p. 259.
15. Harris, S.J. and Weiner, A.M., *Combust. Sci. Technol.* **32**, 267 (1983).
16. Nagle, J. and Strickland-Constable, R.F., *Proceedings of the Fifth Conference on Carbon*, Pergamon, London, 1962, p. 154.
17. Ebert, L.B., Scanlon, J.C. and Clausen, C.A., *Energy & Fuels* **2**, 438 (1988).
18. Wieschnowsky, U., Bockhom, H. and Fetting, F., *Twenty-Second Symposium (International) on Combustion*, The Combustion Institute, 1989, p. 343.

MODELLING THE GROWTH OF POLYNUCLEAR AROMATIC HYDROCARBONS IN DIFFUSION FLAMES

J. Houston Miller
Department of Chemistry
George Washington University
Washington, DC 20052

Damon R. Honnery and John H. Kent
Department of Mechanical Engineering
University of Sydney
NSW 2006, Australia

Abstract

It has been noted for some years that the concentrations of many species in laminar hydrocarbon diffusion flames correlate with mixture fraction, or alternatively, local equivalence ratio. Therefore, once the spatial profile for the mixture fraction is established, it is possible to approximate both the concentration and net chemical rate profiles for a great many flame species. However, some species exhibit concentration gradients along contours of constant mixture fraction in a flame. The results of our past work show that most of the species along the chemical pathway leading to soot particle formation in diffusion flames, including all of the Polynuclear Aromatic Hydrocarbons, exhibit this type of behaviour. For these species, it is necessary to consider not only the chemistry of the growth environment, which may be adequately described by the mixture fraction, but also the residence time within the growth region. This paper will describe how such a model could be expressed, and present some initial comparisons with laboratory flame data.

Introduction

The earliest mathematical treatment of diffusion flame structure was that of Burke and Schumann [1]. Although incremental improvements to the Burke-Schumann model have been made over the years, it was not until recently that a new and more realistic approach to thinking about diffusion flame structure could be formulated. This can be traced to two improvements: the evolution of powerful computers and the development of the conserved scalar description of flame structure. The former has provided the capacity for the calculation of the two-dimensional structure, including up to C_2 chemistry, for laminar diffusion flames. The latter provides a framework for the development of simplification schemes for flame structure calculations.

In general, to compute the structure of a laminar diffusion flame requires the simultaneous solution of the energy, momentum, and species conservation equations. The latter can be written in the Shvab-Zeldovich form as [2]:

$$L(Y_i) \equiv \rho u_k \cdot \left(\frac{\partial Y_i}{\partial x_k} \right) - \frac{\partial \left(\rho D_i \cdot \left(\frac{\partial Y_i}{\partial x_k} \right) \right)}{\partial x_k} = w_i \quad (1)$$

where Y_i is the mass fraction of species i , w_i is its chemical production rate of species i , ρ is the gas density and u_k is the component of velocity in the x_k coordinate.

Chemical elements (such as C, H, and O) are conserved during chemical reaction ($L(Z_i) = 0$) and linear combinations of elemental abundances, such as the mixture fraction, ξ , will also be conserved [3].

It has been noted that the concentrations of many flame species are only a function of mixture fraction, $Y_i = f(\xi)$ [2]. For these species, since

$$\rho u_k \cdot \left(\frac{\partial \xi}{\partial x_k} \right) - \frac{\partial \left(\rho D_i \cdot \left(\frac{\partial \xi}{\partial x_k} \right) \right)}{\partial x_k} = 0 \quad (2)$$

it follows that the chemical rate is given by

$$w_i = - \left(\frac{1}{2} \right) \rho \chi \cdot \left(\frac{d^2 Y_i}{d\xi^2} \right) \quad (3)$$

with the instantaneous scalar dissipation rate, χ , defined as:

$$\chi = 2D \cdot \left(\frac{\partial \xi}{\partial x_k} \right)^2 \quad (4)$$

What if a species concentration is not a function of only mixture fraction? In particular, what if the chemistry is slow enough that transport might occur before a reaction proceeds? This is the case for the species along the chemical pathway leading to soot particle formation in diffusion flames, including all of the Polynuclear Aromatic Hydrocarbons, which exhibit concentration gradients along lines of constant mixture fraction [4]. For these species, it is necessary to consider not only the chemistry of the growth environment, which might be adequately described by the mixture fraction, but also the residence time within the growth region.

If this residence time dependence is included, a more complicated version of Eq. 3 can be derived which has two simple limits. The first would be if the time dependence was zero. In that case the equation would reduce to the result of Eq. 3. The other limit would hold if the diffusion coefficient for the species under consideration were zero, or at least small enough that terms which include it were small with respect to the residence time dependent terms. This would be almost exactly true for soot particles. Even small aromatics have diffusive velocities which are small with

respect to their convective velocities [4]. In this latter limit, the change in a species concentration would be simply given by integration over the residence time. We adopt this simple view in formulating the model presented in the next section.

A Model for PAH Chemistry in Laminar Diffusion Flames

We describe below a model which describes the physical and chemical processes that affect PAH and soot concentrations along a stream line in a laminar methane/air diffusion flame. The development is similar in spirit to that presented in a recent paper by Kennedy et al. [5]. In both models, soot processes are divided into three broad categories: inception, chemical growth, physical growth (agglomeration), and oxidation. Both assume that the rate of the soot processes depends on local temperature and the concentrations of major species, and these are fully determined by mixture fraction. In our model, we attempt to rationalize the choice of rates based on a knowledge of the fundamental chemical processes which are occurring in the flame combined with detailed measurements of species concentrations.

Growth

The growth chemistry in our model is based on the work of Frenklach et al. who proposed a model for ring growth based on the successive addition of acetylene to a growing aromatic radical core [6]. This model, in various forms, has been applied to studies of PAH and soot formation in shock tubes and premixed flames [6-10]. Frenklach developed a simplified version of his model to identify key parameters controlling PAH growth in combustion environments [10]. We used this simplification to demonstrate the important role of agglomeration in PAH growth [11].

In Frenklach's simplified mechanism parent PAH, A_i , are converted into a phenyl-like radical, A_i^- , by hydrogen abstraction. The resulting radical reacts with acetylene to form a radical addition product $A_iC_2H_2^-$. A subsequent acetylene addition irreversibly forms the next largest parent PAH. This reaction sequence is illustrated as:



In this reaction scheme, steady-state estimates for the concentrations of A_i^- and $A_iC_2H_2^-$ can be derived. The rate of formation of the A_{i+1} PAH can therefore be written as

$$\frac{d[A_{i+1}]}{dt} = k_{eff} [A_i], \quad (5)$$

where k_{eff} is dependent upon the concentrations of C_2H_2 , H_2 , and H .

In our prior work, we found that agglomeration only becomes important when the reduced mass of the colliding pair is suitably large: greater than 400 amu. Following the lead of this earlier work, we here assume that an agglomeration reaction can be written as



where the rate constant of this process will be 0 for collisions of lighter PAH and close to the gas kinetic limit for collisions among the heavier PAH.

Inception

As seen above the aromatic growth is treated as an irreversible sequence of acetylenic addition steps to a growing aromatic core whose source is benzene, A_1 . There are a number of

models for the chemistry of the formation process of benzene which involve either reactions of C_2 with C_4 species [6] or the reaction of two C_3 species [15]. It is conceivable that a simplified expression for this process using steady state arguments (analogous to Frenklach's approach for ring growth) might be derived. If successful, such an approach would be expected to result in an expression for the A_1 inception rate which depends only on mixture fraction. However, given the current active debate on the mechanisms for the formation of benzene in flames, such a simplification may be premature.

Fortunately, there may be another approach to deriving an inception rate. Over the past few years we have collected an extensive data base for species concentrations and temperature in a laminar methane/air diffusion flame. This data has included measurements of the concentration of stable species such as acetylene and molecular hydrogen [12] and has been recently extended to include profile measurements of radicals species [13,14]. With this data base, we have demonstrated how the overall rates for a species chemistry may be calculated [13]. For the initial work presented here, we will assume that the benzene formation rate dependence on mixture fraction is given by our previous results for the Wolfhard-Parker diffusion flame [13].

Oxidation

In his dissertation work, McKinnon developed a comprehensive soot model which explicitly included a soot oxidation step [9]. Based on the work of Brezinsky [17], McKinnon assumed that successive reaction of carbons on the PAH or soot with hydroxyl radical results in a decrease of one ring number for the PAH and the formation of carbon monoxide. McKinnon found that inclusion of the Nagle and Strickland-Constable expression for soot oxidation by molecular oxygen overpredicted the soot oxidation rate, and he omitted this pathway from his final model. In the initial steps of the current research, we will also only include oxidation of PAH and soot by hydroxyl radical.

If it is assumed that (1) the concentrations of C_2H_2 , H_2 , H , and OH are only functions of mixture fraction (i.e. their concentrations will not be affected by the aromatic growth chemistry) and (2) aromatic species will not diffuse then the progress of aromatic growth may be followed by integrating aromatic concentrations along a stream line using mixture fraction correlation data from our data base. The derivation of this flame field is discussed in the next section.

Flame Field Calculations

We have modelled the structure of a methane/air diffusion flame which has been studied by Santoro et al. [18]. Velocity, density, and mixture fraction fields throughout the flame are obtained using a computer code which has been described previously [19-21]. In this model, it is assumed that (a) major species concentrations are only a function of mixture fraction (and their concentrations can be found upon solution of the transport equation for mixture fraction, Eq. 2), (b) the rates of chemical reactions that determine major species concentrations are large with respect to transport rates, and (c) all species diffusivities are the same.

The transport equations for mixture fraction and momentum are solved for axisymmetric flow using a streamline coordinate transformation. The flow is parabolic and the boundary layer assumptions are made that the transverse pressure gradient and longitudinal diffusion fluxes are negligible. Buoyancy forces are included in the momentum equation. Diffusivity and viscosity were calculated from the local temperature using the Sandia transport property data [22]. The temperature vs. mixture fraction correlation was obtained from our analysis of a methane/air diffusion flame

supported on a Wolfhard-Parker burner [12]. The predicted mixture fraction field and streamlines are shown in Figure 1.

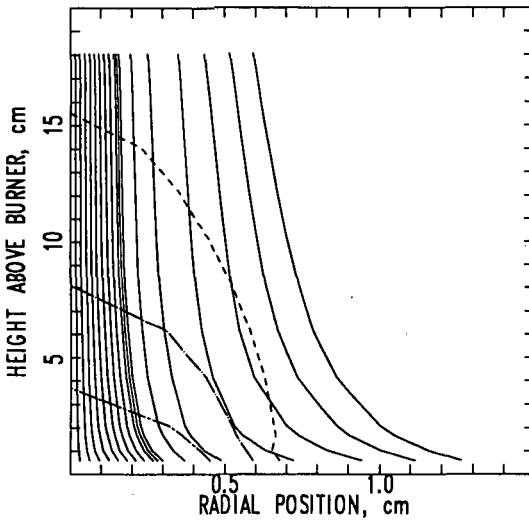


Figure 1 Streamlines and contours of mixture fraction in calculated axisymmetric methane/air diffusion flame. The stoichiometric contour ($\xi = 0.055$), and two fuel-rich contours ($\xi = 0.1$ and 0.2)

Results and Discussion

The concentrations of polynuclear aromatic hydrocarbons have been calculated along a series of streamlines in the flame shown in Figure 1. The model was first run using the expression for the effective rate constant for chemical growth derived from local temperature, and the concentrations of C_2H_2 , H_2 , and $H\cdot$ correlated against mixture fraction from the Wolfhard-Parker flame data. It should be noted that a H -atom plays a critical role in this chemistry: abstraction of ring hydrogens from the PAH is responsible for "activating" the surface for further growth. Unfortunately, in the

flame region that growth is likely to occur, there are no reliable measurements of H-atom concentration [14]. In these flame regions we have calculated [H·] assuming total local equilibrium. There has been much written about the importance of super-equilibrium concentrations of radicals in combustion processes in general [19] and aromatic growth in particular [10]. Although it is well known that super-equilibrium exists near the high temperature reaction zone of hydrocarbon diffusion flames [13], calculations also suggest that super-equilibrium extends well into the fuel rich flame regions where growth may occur [19]. Therefore, assumption of total equilibrium may grossly underpredict the concentration of hydrogen atoms and, consequently, the rate of ring growth. Our model calculations bear this out: unless an enhancement factor for chemical growth was included, no appreciable build-up of PAH occurs. To reach a volume fraction of soot approaching that which has been observed experimentally [18], this factor must be on the order of 500, which implies hydrogen atom concentrations in the growth region on the order of a few hundred parts per million. With current measurement strategies for hydrogen atom, this is a value near the detection limit in fuel rich regions of a diffusion flame [23].

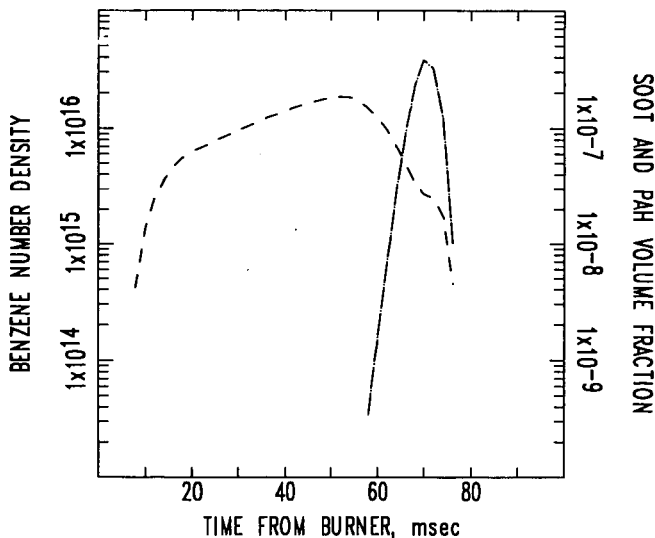


Figure 2 Concentrations of benzene (—) and heavy PAH and soot (---) as a function of time from burner surface for the streamline of peak soot loading (the fifth from the right streamline in Figure 1).

Figure 2 shows the concentrations of benzene and the soot volume fraction along a streamline which exhibited maximum PAH growth rates. Soot volume fraction is defined as the volume occupied by all species larger than coronene (A_7) in the model assuming that they all have the same density as soot. As expected, large concentrations of benzene precede the formation of larger PAHs in the

flame and that the volume fractions in this flame are small enough that total oxidation of the PAH occurs near the flame tip. (The oxidation of larger PAH leads to the shoulder on the benzene profile at 70 msec.)

Figure 3 shows a contour plot for soot concentrations in the flame calculated with the factor of 500 used for the enhancement of chemical growth rates. This picture looks qualitatively similar to comparable pictures derived from laser light scattering and extinction measurements [18] and to other model calculations of soot formation and oxidation in diffusion flames [5].

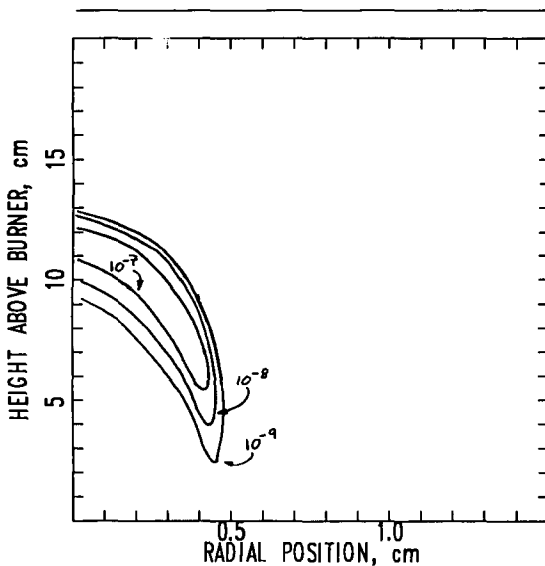


Figure 3 Contours of soot volume fraction in methane/air diffusion flame.

Conclusions

These model calculations provide an initial attempt to combine simplified aromatic growth chemistry with the conserved scalar description of diffusion flame structure. Although preliminary, the results suggest the important role that super-equilibrium hydrogen atom concentrations play in the growth chemistry. Future model improvement will hinge on the development of a more quantitative understanding of this factor.

Acknowledgments

One of us (JHM) would like to thank the English Speaking Union for the Churchill Fellowship Award that led to this collaboration and the Building and Fire Research Laboratory of the National Institute of Standards and Technology for continued support of this research.

References

1. Burke, S.P. and Schumann, T.E.W., *Industr. Engng. Chem.* 20, 998 (1928).
2. Bilger, R.W., *Combust. Flame* 30, 277 (1977).
3. Bilger, R.W., *Ann. Rev. Fluid Mech.* 21, 101 (1989).
4. Hamins, A., Anderson, D. and Miller, J.H., *Combust. Sci. Technol.* 71, 175 (1990).
5. Kennedy, I.M., Kollmann, W. and Chen, J.-Y., *Combust. and Flame* 81, 73 (1990).
6. Frenklach, M., Clary, D.W., Gardiner W.C., Jr. and Stein, S.E., *Twenty-First Symposium (International) on Combustion*, p. 1067, The Combustion Institute, 1986.
7. Frenklach, M. and Warnatz, J., *Combust. Sci. and Tech.* 51, 265 (1987).
8. Harris, S.J., Weiner, A.M. and Blint, R.J., *Combust. and Flame* 72, 91 (1988).
9. McKinnon, J.T., Jr., Ph.D. Dissertation, Massachusetts Institute of Technology, 1989.
10. Frenklach, M., *Twenty-Second Symposium (International) on Combustion*, p. 1075, The Combustion Institute, 1989.
11. Miller, J.H., *Twenty-Third Symposium (International) on Combustion*, The Combustion Institute, in press.
12. Smyth, K.C., Miller, J.H., Dorfman, R.C., Mallard, W.G. and Santoro, R.J., *Combust. Flame* 62, 157 (1985).
13. Smyth, K.C., Tjossem, P.J.H., Hamins, A. and Miller, J.H., *Combust. and Flame* 79, 366 (1990).
14. Smyth, K.C. and Tjossem, P.J.H., *Twenty-Third Symposium (International) on Combustion*, The Combustion Institute, in press.
15. Stein, S.E., Walker, J.A., Suryan, M.M. and Fahr, A., *Twenty-Third Symposium (International) on Combustion*, The Combustion Institute, in press.
16. Miller, J.H., Mallard, W.G., and Smyth, K.C., *Twenty-First Symposium (International) on Combustion*, p. 1057, The Combustion Institute, 1986.
17. Brezinsky, K., *Prog. Energy Combust. Sci.* 12, 1 (1986).
18. Santoro, R.J., Yeh, T.T., Horvath, J.J. and Semerjian, H.G., *Combust. Sci. and Tech.* 53, 89 (1987).
19. Bilger R.W. and Stårner, S.H., *Combust. and Flame* 51, 155 (1983).
20. Honnery, D.R. and Kent, J.H., *Combust. and Flame* 82, 426 (1990).
21. Kent, J.H. and Honnery, D.R., *Combust. Sci. and Tech.* 54, 383 (1987).
22. Kee, R.J., Miller, J.A. and Jefferson, T.A., *Sandia National Labs. Report SAND80-8003*, (1980).
23. Smyth, K.C., personal communication.

MOLECULAR-BEAM STUDIES OF CARBONACEOUS CLUSTERS*

Thomas J. Butenhoff and Eric A. Rohlfing
Combustion Research Facility
Sandia National Laboratories
Livermore, CA 94551

Keywords: Carbon and carbonaceous clusters, soot formation.

INTRODUCTION

Carbon clusters ranging in size from a few to a few hundred atoms are currently a topic of intense theoretical and experimental study. Recent advances have made it possible to synthesize C_{60} , buckminsterfullerene, and other even-numbered carbon clusters ("fullerenes") in macroscopic quantities so that these spherical clusters, and their chemical derivatives, have made the leap from laboratory curiosities to potentially important materials. This has led to an explosion of research in fullerene characterization and chemistry. Fullerenes are ubiquitous to a variety of growth environments that abound in species with elements other than carbon and are implicated in environments ranging from sooting flames to interstellar space. Fullerene ions can be observed as the dominant mass spectral features when a variety of substrates, including polycyclic aromatics,¹ polymers,² and soot particles,³ are vaporized by a laser *in vacuo*. They are also observed in sooting flames in the region where soot particles first form.^{4,5}

No matter what the conditions of growth, it now seems clear that the fullerenes and carbon (or soot) particles are intimately connected. At question is the model for particle growth proposed by Kroto^{6,7} and Smalley⁸ that has been postulated to account for the molecular beam results and has been extended to explain soot formation in combustion. Simply put, this model assumes that the nucleus of the growing particle is an incomplete spherical shell that accumulates primarily graphitic carbon on its reactive edges. A fullerene is formed in the rare event that a shell closes, thereby becoming inert with respect to further growth. This model has been the subject of much debate⁹ between its proponents and those who favor the more traditional mechanism for soot formation. The traditional view¹⁰⁻¹² explains the rapid growth of soot at its inception by reactions between large polycyclic aromatics that are found in abundance in sooting flames. Subsequent addition of mass then proceeds via surface growth reactions between the soot particle and smaller gas phase reactants. The observation of fullerenes in sooting flames by Homann et al.^{4,5} has been taken by some as evidence for the spiraling shell model. However, Homann et al. interpret their results within the traditional mechanism and hypothesize that the fullerenes are formed from nascent soot particles by an evaporative process.

We have begun a program to study the reactions of large carbon clusters and their hydrogenated analogs, which we shall call carbonaceous clusters, and attempt to make the connection between the molecular beam/flow reactor environment and a sooting flame. Smalley and co-workers have previously examined the reactivities of small ($n < 20$) and large ($n > 40$) carbon clusters in molecular beam work with the laser vaporization clusters source. In one study, Heath et al.¹³ looked at the C_n and C_nH_m ions produced by the multiphoton ionization of neutrals created by the addition of various hydrogen-containing reactants to the carrier gas upstream of the laser-induced plasma. In another study, Zhang et al.⁸ examined the reactivities of the large neutral clusters in a fast flow reactor located downstream of the vaporization region; they used single-photon ionization to probe the neutral cluster distributions. These experiments showed the unique inertness of the fullerenes to chemical attack by a variety of reactants. In both these studies, the authors used a linear time-of-flight mass spectrometer (TOF MS) with moderate mass resolution. In particular, the mass resolution in the fullerene study was insufficient to observe the products of the facile reactions between the injected reactant and the

* This work supported by the United States Department of Energy, Office of Basic Energy Sciences, Chemical Sciences Division.

odd-numbered clusters (which cannot achieve closed shells). These products appeared as an unresolved background from which the fullerene peaks stood out.

In this paper, we summarize results from experiments in which the formation of clusters is modified by addition of hydrogen to the carrier gas that flows over the graphite in the laser-vaporization source.¹⁴ The resulting carbon and carbonaceous clusters (for $n \geq 20$) are gently single-photon ionized by a vacuum ultraviolet laser (F_2 158 nm) in order to probe the neutral cluster distribution without extensive perturbation from ionization efficiency or multiphoton fragmentation. The cluster ions are subsequently mass analyzed in a high resolution reflectron TOF MS. The resolution of this instrument at high mass ($M/\Delta M \sim 1700$ at 720 amu) allows us to completely resolve mass peaks separated by 1 amu, i.e. each value of m in C_nH_m . By adjusting the growth conditions in the cluster source through combinations of carrier gas density and residence times, we can produce carbon cluster distributions that exhibit wide variations in their degree of local maxima, or magic numbers. For example, we find low-growth conditions in which the abundances of odd clusters are nearly equal to those of the fullerenes. Alternatively, we can create very "magic" distributions in which the fullerenes, especially C_{60} , dominate the neighboring odd clusters. The carbonaceous cluster distributions produced by the addition of hydrogen to the carrier gas always show a dramatic preference for the formation of C_nH_m clusters with odd n . Remarkably, the clusters with even n appear predominantly as pure C_n , i.e. the fullerenes. We quantify these qualitative trends through a hydrogenation analysis that determines the fraction of each cluster that is hydrogenated and the distribution of hydrogens among the C_nH_m . The quantitative results (hydrogenation fraction, hydrogenation distribution, C/H ratio, etc.) show vivid evidence for the formation of long polyacetylenes, C_nH_2 , for even n up to $n=44$. In addition, they reveal a dramatic change in hydrogenation behavior at about $n=40$ that provides more indirect evidence in support of the fullerene structural hypothesis. Finally, we discuss the implications of our results with respect to incomplete spherical shells and the corresponding model for particle growth.

EXPERIMENTAL TECHNIQUE

Carbon clusters are created by laser vaporization of graphite (3.2-mm-diameter rod, Pure Tech, 99.99%) into the helium flow following a piezoelectrically actuated pulsed valve that operates with 10-100 psig backing pressure and a 1-mm-diameter orifice. The vaporization laser is the second harmonic of a Nd:YAG laser (Spectra Physics DCR-11) at 532 nm with a pulse length of 6-7 ns and energy of 17 mJ. The flow channel is 2.5 mm in diameter at the target rod and for 22 mm downstream; the last 12 mm of the channel forms a 30° conical nozzle from which the flow expands into a vacuum chamber pumped by an unbaffled diffusion pump (Varian VHS-10). The cluster/helium expansion is skimmed once in the source chamber (5-mm-diameter skimmer, Beam Dynamics) at 35 cm downstream of the source. The resulting molecular beam enters a second vacuum chamber pumped by a 500 l/s turbomolecular pump (Balzers TPU 510) and is further collimated by a second 5-mm skimmer (98 cm downstream) before entering the ionization chamber of the reflectron TOF MS, which is located 109 cm downstream of the source. Carbonaceous clusters, of the generic formula C_nH_m , are formed in the same manner as C_n except that the helium carrier gas is replaced by a mixture of H_2 in helium. Vacuum ultraviolet photoionization using the light from an excimer laser (Questek 2820) operated on the F_2 line at 158 nm (7.89 eV) creates cluster ions in the ion source of the reflectron TOF MS. Typical laser pulse length and fluence are ~ 17 ns and 0.1 mJ/cm², respectively. The timing for these experiments is controlled by two digital delay generators (SRS DG535) under computer control.

The reflectron TOF MS is a modified version of a commercially available instrument (R. M. Jordan Co.) and is arranged such that the initial ion-beam axis is collinear with the neutral cluster beam. The repeller-extractor and extractor-ground plate spacings are 1.9 cm and 0.95 cm, respectively; the repeller and extractor voltages are 1800 V and 1000 V, respectively. The ion beam (nominal energy 1400 eV) is accelerated out of the ionization source along the neutral beam for 0.5 cm before entering a static deflection field of 37 V/cm that extends for 3.8 cm. This field deflects the ions over a total angle of 7.2°. After passing the first flight region (97.7 cm), the ions are decelerated and re-accelerated in a two-stage reflector. The first stage is defined by two gridded plates separated by 1.2 cm and has a 1000 V potential increase. The second stage is

9.7 cm long and consists of 11 guard rings with elliptical openings terminated by the reflector plate. Final temporal focusing of the ions is achieved by fine adjustments of the electric field in the second stage by changing the voltage applied to the reflector plate (nominally 1620 V). Ions emerging from the reflector traverse the second field-free flight region of 64.2 cm in length before striking a 40-mm-diameter dual microchannel plate detector (R. M. Jordan Co.). The ion time-of-flight signals are amplified (Comlinear CLC 100) and digitized by a 400 MHz digital oscilloscope (LeCroy 9450). The TOF mass spectrum is acquired as separate summation averages (typically 1000 laser shots) in 50- μ s increments and is transferred from the digital oscilloscope to a host computer for analysis.

RESULTS

A. Mass Spectra

In Fig. 1 we display an example of the TOF mass spectrum of C_nH_m ions for $n=16-160$ obtained under moderate-growth source conditions with a 0.5% H_2/He mixture. We have taken many other C_n and C_nH_m mass spectra under low-growth and high-growth source conditions.¹⁴ Our definitions of the growth characteristics in the cluster source are predicated on the nature of the carbon-cluster mass spectrum taken under identical detection conditions. We define "low-growth" conditions as those under which the odd-numbered C_n are roughly as abundant as the even-numbered clusters in the region near $n=60$. A distribution near $n=60$ in which the even clusters, and particularly C_{60} , have considerably more intensity than the odd clusters defines "moderate growth" (see Fig. 1). For our cluster source with the flow channel described above, moderate growth is the norm, i.e. 100 psig backing pressure, full driving voltage applied to the valve, and vaporization timed to occur in the center of the gas pulse. Low growth can be achieved in several different ways: lowering the backing pressure to 10 psig, lowering the driving voltage on the piezoelectric valve, or by firing the vaporization laser early in the gas pulse. All of these approaches lower the effective density of the carrier gas over the target when the vaporization laser fires. We can also achieve high-growth conditions, in which C_{60} completely dominates the C_n distribution at $50 \leq n \leq 70$, by running under nominal conditions and increasing the length of the flow channel by 27 mm. The observation of enhanced even/odd alternation with increasing carrier gas in the source is consistent with the model proposed by Smalley and Kroto in which the fullerenes are the survivors of the cluster-growth process that ultimately leads to carbon particles. Increasing the carrier gas density provides greater containment of the carbon vapor in the laser-induced plasma and thus provides a higher density of growth species and leads to more rapid condensation.

The moderate-growth mass spectrum produced with a 0.5% H_2/He mixture in Fig. 1 shows hydrogenated clusters, C_nH_m , that appear both with n even and odd up to about $n=40$. At this point the odd clusters continue to appear predominantly as hydrogenated species while substantial intensities of even C_n appear above this hydrocarbon "soup". Figure 2 displays the comparison of the C_n and C_nH_m moderate-growth mass spectra for $n=21-24$ and $n=58-62$. For a given n , the signal for each mass peak in the C_nH_m spectrum has contributions from the ^{13}C isotopic variants of C_n and from the C_nH_m species and their ^{13}C isotopic variants. This convolution, which increases in severity with increasing n because the ^{13}C distribution widens, makes it impossible to determine the distribution of hydrogenated species directly from the mass spectrum. Note the propensity for the formation of C_nH_2 for the even-numbered clusters in the $n=21-24$ range. The C_nH_m spectrum for $n=58-62$ in Fig. 2 shows hydrogenation of both even and odd clusters near $n=60$. However, the extent of the hydrogenation is clearly much greater for the odd clusters; substantial amounts of the even clusters appear as bare carbon clusters. In the low growth case, the addition of hydrogen enhances the appearance of the even C_n , and especially C_{60} , with respect to the hydrocarbon background. Remarkably, this occurs even when the even clusters do not appear as "special" in the corresponding C_n spectrum.

B. Hydrogenation Analysis

To quantify the extent of hydrogenation and the distribution of hydrogen atoms for C_nH_m at a given n , we have developed a procedure in which the effects of the ^{13}C isotopic distribution are deconvoluted from the hydrogenation distribution. Ref. 14 describes this procedure in detail.

It is applicable to situations in which the hydrogenation distribution for cluster n ends before the one for cluster $n+1$ begins, i.e. $m \leq 11$. For the data presented here, we can apply the deconvolution to the moderate-growth spectrum over the entire range of n in which sufficient mass resolution is maintained (typically $n \leq 100$). From the analysis we extract the hydrogenation fraction, x_h , and the fractional abundance for each m , g_m .

One of the more dramatic effects, discussed qualitatively above, that we observe in the carbonaceous cluster distributions is the tendency for the even clusters above $n=40$ to appear as bare C_n while the odd clusters are hydrogenated. This effect is shown vividly in Fig. 3 in which we plot the hydrogenation fraction, x_h , versus cluster size, n , for the moderate-growth experiment. At low n both odd and even clusters show hydrogenation fractions that are high, 75-90%. At about $n=40$ there is a sharp drop in x_h for the even clusters while the hydrogenation fraction for the odd clusters stays high, never dropping much below 80%. The hydrogenation fraction is lowest for the even clusters in the $n=50-70$ range with a sharp minimum at $n=60$. The dramatic odd/even alternation near $n=60$ is shown quite nicely in the mass spectrum (Fig. 2); only 34% of the $n=60$ peak corresponds to $C_{60}H_m$ while 85% of the neighboring $n=61$ peak is due to hydrogenated species. Above $n=70$ the hydrogenation fraction gradually increases for even n and decreases for odd n , with the two curves apparently heading toward a common asymptote. This trend cannot be confirmed in this data because of the loss of mass resolution at $n > 100$.

We can quantify the tendency for even C_nH_m to appear with $m=2$ by examining the ratio of the fractional abundances for $m=2$ and $m=1$, g_2/g_1 . Fig. 3 displays a plot of g_2/g_1 versus n for the moderate-growth data. For the odd clusters this ratio stays constant at or near unity until around $n=70$. By contrast, g_2/g_1 is much larger for the even clusters until it drops quickly near $n=40$ so that for $n \geq 46$ the ratio is nearly identical for both odd and even clusters. This data demonstrates that with small amounts of hydrogen present in the source clusters as large as $n=44$ have a decided preference to appear as C_nH_2 ; odd clusters show no such preference. Near $n=60$, both even and odd clusters show a hydrogenation distribution that decreases monotonically with m and thus $g_2/g_1 < 1$. As n increases above about 70, the distributions widen and develop maxima at $m > 1$ so that the ratio g_2/g_1 gradually rises to values larger than unity.

DISCUSSION AND CONCLUSIONS

The mass spectra of C_nH_m ions for $8 \leq n \leq 20$, produced by multiphoton ionization of neutrals made by addition of various reactants to the carrier gas, have been discussed by Heath et al.¹³ They also observe the tendency for even clusters to form C_nH_2 species while the odd numbered clusters generally are found to have no distinctive hydrogenation pattern. The formation of C_nH_2 species is a strong signature of linear polyacetylenes of the form $H-C \equiv C-(C \equiv C)_m C \equiv C-H$. Heath et al. postulate that these form by the addition of two hydrogens to the terminal carbons of linear carbon chains that are triplet diradicals, $\cdot C \equiv C-(C \equiv C)_m C \equiv C \cdot$. Our data extends the results of Heath et al. to larger clusters. Interestingly, we observe a preference for C_nH_2 formation for even clusters up to $n=44$. This preference demonstrates that at least some of the C_nH_m species formed in our experiments are very long polyacetylenes. For $n \geq 10$ theoretical calculations for bare carbon clusters agree that monocyclic rings are more stable than linear chains. However, for reasons we now explore, it seems highly unlikely that long polyacetylenes are formed by hydrogenation of existing monocyclic rings.

In this type of experiment, where H_2 is added to the carrier gas upstream of the laser-induced plasma, we interpret the results in terms of a modification of the cluster growth that occurs without the reactant gas. The most important hydrogenation reactions are probably facile radical-radical reactions, i.e. reactions between H atoms and carbon or carbonaceous radicals. The results of Heath et al. support the assertion that H-atom reactions are important; they observe similar C_nH_m products for a variety of hydrogen-containing reactants.⁸ Under our experimental conditions the carbon density in the vaporization plume is in great excess of the H-atom concentration and carbon-cluster growth via reactions with small growth species (C , C_2 , and C_3) will proceed largely as if there was no reactant gas. The important difference is that hydrogen atom attack on a radical center might now render a cluster relatively inert with respect to further growth or hydrogenation. For even clusters with less than about 44 atoms this is observed as the formation of long polyacetylenes, the first non-radical species that can be formed

for a linear geometry. It is important to note that H-atom attack on a radical center might occur at any point in the cluster growth, not just at the end. For example, a linear C_{10} might be terminated at one end but continue to grow via carbon addition at the other, reactive end until it also encounters an H atom and is terminated.

The same picture of the modification of cluster (and ultimately particle) growth can be used to interpret our results for the larger carbonaceous clusters ($n \geq 40$). The results of our hydrogenation analysis of the data taken under moderate-growth conditions show dramatically the change in nature of the carbon and carbonaceous clusters near $n=40$. The plots of hydrogenation fraction and the ratio g_2/g_1 versus cluster size (Fig. 3) are particularly vivid in this regard. This pronounced change in behavior must be associated with a global change in geometric structure. Near $n=40$ the evidence for linear polyacetylenes disappears and the even clusters become inert relative to their odd neighbors. Clearly, even-numbered can adopt structures that do not have reactive, radical centers, i.e. closed shell fullerenes. By contrast, the odd clusters always appear hydrogenated, since they can only eliminate dangling bonds by hydrogenation.

As with the smaller clusters, the addition of hydrogen to the source in our experiments produces a relatively small perturbation in the overall growth of clusters and particles. One possible effect is that the H atoms in the cluster-growth region might decrease the likelihood of shell closure by tying up the radical sites at the edges of spiraling shells. However, the addition of hydrogen always accentuates the appearance of the fullerenes through the preferential hydrogenation of the neighboring odd clusters. This effect is especially pronounced in the low-growth spectra. On the basis of the low-growth C_n distribution alone, one might infer that both even and odd clusters are unclosed, reactive isomers, i.e. the even clusters have not yet found their way to closure. Yet, the addition of hydrogen under low-growth conditions clearly shows that some of the even clusters have already closed and become unreactive.

The implication of these results is that cluster growth and cluster hydrogenation are at least partially separable processes, with growth preceding hydrogenation. As noted above, it is dangerous to interpret our experiments entirely in this manner since hydrogen is present at all times in the course of cluster growth. However, such behavior can be rationalized both on fluid dynamic and thermodynamic grounds. Large clusters, and even particles, grow rapidly in the vaporization plume where the concentration of growth species in the carbon vapor is high relative to the hydrogen reactant. Significant hydrogenation may not take place until the vaporization plume is mixed by turbulence with the reactant/carrier gas mixture at points downstream. Also, in the high-temperature vapor plume the graphitic, spiraling shells are thermodynamically favored over their hydrogenated analogs. As the temperature drops during the flow through the source, irreversible hydrogenation of reactive sites can produce carbonaceous clusters. The even clusters can adopt closed structures under high-temperature pyrolytic conditions and thus become inert to subsequent hydrogenation at lower temperatures. By increasing the carrier gas density to our moderate-growth conditions, we drive the condensation process harder by increasing the carbon density in the high-temperature region, thereby allowing more even clusters to become fullerenes. Addition of small amounts of hydrogen under these conditions effectively "titrates" the odd clusters by hydrogenation but the unreactive even clusters emerge largely unscathed (see Fig. 2).

The conditions in our experiments are intentionally adjusted in order to avoid extensive hydrogenation. The relatively small amount of hydrogenation is thus insufficient to tie up all the reactive sites in a growing cluster and substantially slow further growth toward particles. The C/H ratio for the C_nH_m species that we produce in the moderate-growth experiment increases monotonically from ~ 6 at $n=20$ to ~ 18 at $n=100$. These values are much higher than what one would expect for spiraling shells whose reactive edges were completely saturated with hydrogens. As an upper bound on the C/H ratio of such species, consider the series of D_{6h} polycyclic aromatics of the form $C_{6j}H_{6j}$, i.e. C_6H_6 , $C_{24}H_{24}$, $C_{54}H_{54}$, $C_{96}H_{96}$, etc. The C/H ratio in these planar species is simply j ; the C/H ratio is 3 at $n=54$ and 4 at $n=96$. Generally, a partially closed shell will have fewer possibilities for C-H bonds than these species. A reasonable estimate might be a shell with half as many reactive sites; this gives a C/H ratio of 6-8 for $n=54-96$. We observe a C/H ratio of 15-20 in this size range in our moderate growth

experiment. This indicates that the hydrogenation distributions are still in the kinetically limited regime and do not represent saturation of all reactive sites. Finally, we note that our carbonaceous clusters are more carbon-rich than soot particles formed in combustion processes. Typically, nascent soot particles have a C/H ratio of 2-3 that may increase to 8-10 as the soot dehydrogenates at later stages in the flame.¹⁰

Our results, in which we study the formation of carbon and carbonaceous clusters in a laser-vaporization source with controlled addition of hydrogen, are quite similar to those obtained in a variety of other *in vacuo* laser vaporization studies¹⁻³ and in the flame studies of Homann et al.^{4,5} In all these cases, the large, even carbon clusters appear as the dominant mass spectral feature under conditions where there are substantial quantities of elements, especially hydrogen, other than carbon in the growth region. In our controlled hydrogenation studies we create conditions in which the neighboring odd clusters form a hydrocarbon background against which the fullerenes appear. We suspect that in some of the other vaporization studies and flame investigations the fullerenes stand out from a similar, unresolved hydrocarbon background, although the hydrogenation may be more extensive and thus spread the cluster distribution over a wider mass range. The idea that rapid carbon-cluster growth, and occasional fullerene shell closure, occurs in high-temperature regions where hydrogenation, or oxidation, is not favored must also apply to these environments. In the laser vaporization experiments, the high-temperature region is the laser-induced, high density plasma formed above the substrate, whether it be soot³ or various polymers.² In the flame studies, the fullerenes are found in the region where the temperature is near its maximum ($T \sim 2100$ K) and soot particles first begin to form.^{4,5} The exciting and unanswered question in these experiments is whether the fullerenes are created during soot formation, as proposed by Smalley and Kroto, or as the result of vaporization from the surface of a soot particle, as hypothesized by Homann et al.⁵

One of the great difficulties in elucidating the mechanism of soot inception is that the species one observes in a sooting flame, whether they be polycyclic aromatics or fullerenes, are the by-products of the process. The keys to any chemical mechanism are to be found in the radical species that control the kinetic pathway. Unfortunately in the case of soot formation, these radicals wind up buried in the soot particles; the manner in which they arrived there is but a distant memory. Analysis of the particles, while informative, cannot provide the data necessary to differentiate between hypothetical formation pathways.

In the future, we shall investigate the role of large carbonaceous clusters in soot inception and growth by concentrating on reaction studies of the reactive clusters. These may be the odd clusters, which can never completely close, or the reactive isomers of the even clusters. The cluster beam source provides an ideal forum for studies of reactive intermediates because these species can be frozen out in the free jet expansion. We shall perform more studies, such as those presented here, in which reactants are added upstream of the vaporization. Of particular interest is the formation of carbonaceous clusters under conditions that emulate those in a sooting flame, i.e. oxidative, not just pyrolytic. In addition, we shall pursue more controlled chemical reactions using the fast-flow reactor techniques that have been used so successfully in the study of metal cluster chemistry. Zhang et al. have performed some initial work in this area on the large carbon clusters.⁸ However, their study was aimed principally at the unique, unreactive nature of the fullerenes; the products of reactions with odd clusters were observed only as unresolved background. We intend to use the high resolution of the reflectron to sort out the products of reactions such as $C_nH_m + C_2H_2$, which represents a model for the growth of a soot particle through the addition of acetylene. Again, the emphasis will be on arresting the growth process in order to examine clusters that are reactive intermediates and not on the stable by-products, such as the fullerenes.

References

1. D. N. Lineman, K. V. Somayajula, A. G. Sharkey, and D. M. Hercules, *J. Phys. Chem.* **93** (1989) 5025.
2. W. R. Creasy and J. T. Brenna, *J. Chem. Phys.* **92** (1990) 2269; W. R. Creasy and J. T. Brenna, *Chem. Phys.* **126** (1988) 453.
3. H. Y. So and C. L. Wilkins, *J. Phys. Chem.* **93** (1989) 1184.

4. Ph. Gerhardt, S. Löffler, and K. H. Homann, *Chem. Phys. Lett.* **137**, 306 (1987).
5. Ph. Gerhardt, S. Löffler, and K. H. Homann, *Twenty-Second Symposium (International) on Combustion*, p. 395 (The Combustion Institute, 1989).
6. H. W. Kroto, *Nature* **329**, 529 (1987).
7. H. W. Kroto and K. McKay, *Nature* **331**, 328 (1988).
8. Q. L. Zhang, S. C. O'Brien, J. R. Heath, Y. Liu, R. F. Curl, H. W. Kroto, and R. E. Smalley, *J. Phys. Chem.* **90**, 525 (1986).
9. R. M. Baum, "Ideas on Soot Formation Spark Controversy," *Chem. and Eng. News*, February 5, 1990, p. 30.
10. S. J. Harris and A. M. Weiner, *Ann. Rev. Phys. Chem.* **36**, 31 (1985).
11. K. H. Homann, *Twentieth Symposium (International) on Combustion*, p. 857 (The Combustion Institute, 1984).
12. H. GG. Wagner, *Seventeenth Symposium (International) on Combustion*, p. 3 (The Combustion Institute, 1979).
13. J. R. Heath, Q. Zhang, S. C. O'Brien, R. F. Curl, H. W. Kroto, and R. E. Smalley, *J. Am. Chem. Soc.* **109**, 359 (1987).
14. E. A. Rohlfing, *J. Chem. Phys.* **93**, 7851 (1990).

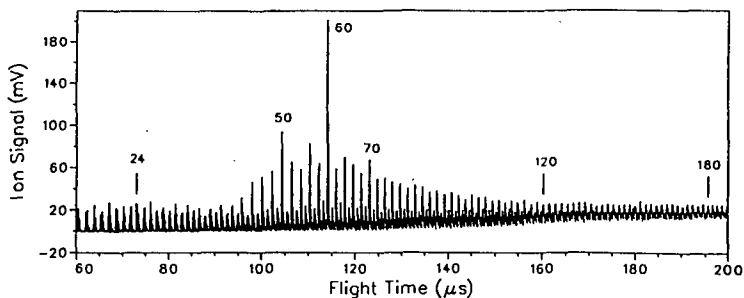


FIG 1. Reflectron TOF mass spectrum of carbonaceous clusters, C_nH_m , produced with a 0.5% H_2/He mixture as the carrier gas under moderate-growth conditions in the cluster source.

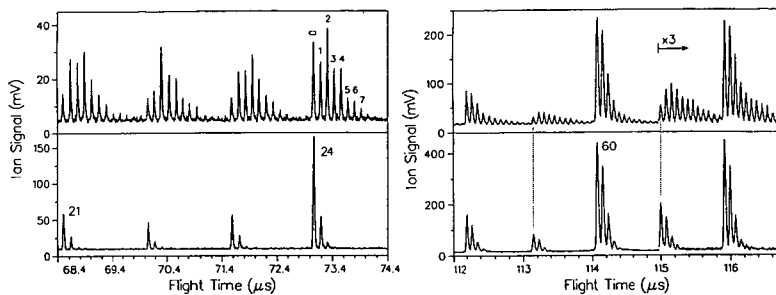


FIG. 2. Close-up views ($n=21-24$ and $n=58-62$) of the C_n and C_nH_m mass spectra taken under moderate-growth conditions. Top panels: spectra of C_n taken with He carrier gas; bottom panels: spectra of C_nH_m taken with 0.5% H_2 /He carrier gas.

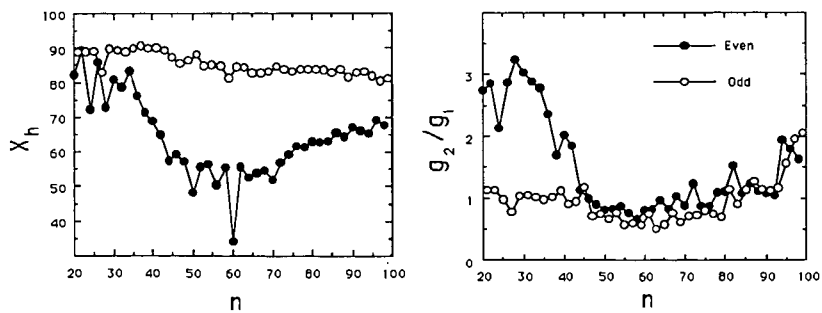


FIG. 3. Results of hydrogenation analysis for moderate-growth C_nH_m mass spectrum (Fig. 1) as a function of cluster size, n . Left: the fraction of hydrogenated species. Right: the ratio of fractional abundances of for $m=1$ and $m=2$.

Polycyclic Aromatics, Fullerenes and Soot Particles
as Charged Species in Flames

Th. Baum, S. Löffler, P. Weilmünster and K. H. Homann
Institut für Physikalische Chemie, Technische Hochschule Darmstadt
Petersenstr.20, D-6100 Darmstadt

1. INTRODUCTION AND EXPERIMENTAL

The ionic structure of fuel-rich hydrocarbon flames resembles the profiles of the larger neutral intermediates much more than those of initial reactants and main products. This applies in particular to polycyclic aromatic hydrocarbons (PAH). They have low and rather similar ionization potentials and relatively large proton affinities. The pattern of reactions of positive ions, condensation and cyclization reactions, shows many similarities with the behavior of their neutral counterparts. Apart from the predominance of some PAH⁺ with an odd number of C atoms, which would be radicals in the neutral state, the occurrence of PAH⁺ is an indication of the existence of the respective neutral compounds. Thus, large flame ions, their composition, reactions and equilibria at high temperature are not only of interest for themselves, but also reflect the existence and behavior of large neutral PAH. The discussion of fullerenes in flames has still to be based solely on their ions.

The experimental procedure of sampling 26.6-mbar flat premixed flames via a two-stage nozzle/molecular beam sampling system and analyzing the ions by a time-of-flight MS has been reported [1, 2]. Recently, the MS was modified by adding a Mamyrin-type ion reflector, thereby increasing the mass resolution $(m/\Delta m)_{\text{exp}}$ to about 1500. The flight time was determined by a multi-stop time-to-digital converter. Ion signals from about 20.000 extraction pulses were summed up to give the mass spectrum. Details will be published elsewhere [3].

2. POLYCYCLIC AROMATIC HYDROCARBON IONS (PAH⁺)

The main formation of the PAH⁺ in sooting flames takes place in the oxidation zone where their concentrations go through maxima (Fig. 1) [2]. The decrease of the PAH⁺ with $m < 325$ u after their maxima is due to thermal decomposition, probably initiated by oxidative attack. It takes place almost simultaneously for these lower-mass PAH⁺. The larger PAH⁺ with $m > 325$ u continue to grow as shown by the shift of their maxima to greater heights with increasing mass. The largest PAH⁺ in acetylene flames reach masses of about $2.5 \cdot 10^3$ u.

PAH⁺ occur with any number of C atoms and those with a certain carbon content contain a varying number of hydrogen atoms (Fig. 2). The number of H atoms points to certain structures. Other arguments in this respect are the thermal stability, the relation to identified neutral PAH and the occurrence of certain side chains, the prevalence of peri-condensation and the possibility of protonation and deprotonation as a function of temperature.

The relatively large concentration of C₁₃H₉⁺ in C₂H₂ flames, an indication of little reactivity, is a strong argument for the stable fully condensed phenalenylium (I):



(I)



(II)

Other isomers such as (II) would be less stable. The far less thermally stable dihydro-compound, $C_{13}H_{11}^+$, occurs in extremely low concentration. At higher temperature, $C_{13}H_7^+$ is formed, an ion that cannot be formulated as a tricyclus without assuming a benzyne bond which was never observed in flame components. A more probable structure, compatible with structural elements normally found in PAH, would be:



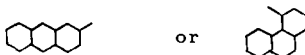
It could be formed by thermal decomposition from phenalenylium via retro-insertion out of a six-membered ring followed by H_2 elimination from the resulting side chain. Structures with side chains

containing triple bonds are suggested for the relatively hydrogen-poor PAH⁺ with $m \lesssim 300$ u. It is known from butadiyne pyrolysis that such side chains are split off from PAH at temperatures $\gtrsim 1400$ K [4]. This would fit the finding that the lower-mass PAH⁺ decompose thermally in a flame zone where polyne ions are formed.

A $C_xH_{y+2}^+$, being present in appreciable concentration compared to a main PAH⁺ $C_xH_y^+$, indicates a change in the carbon skeleton rather than hydrogenation. For $C_{15}H_9^+$ probable structures are

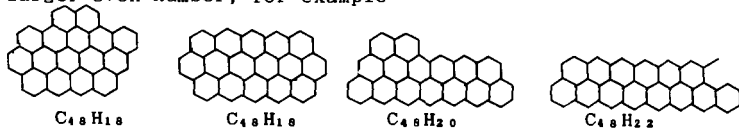


while $C_{15}H_{11}^+$ is rather a tricyclus with a CH_2 group

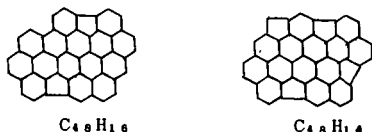


Protonation enlarges the variation in the number of H atoms of even-numbered PAH⁺ without change in the carbon skeleton (Fig. 2). Another example is the C_{16} -PAH which is present as $C_{16}H_{11}^+$ (protonated pyrene or less probable fluoranthene, closed-shell ions) and $C_{16}H_{10}^+$ (ionized pyrene, radical ion). At lower temperature the protonated PAH is formed, but at higher temperature the latter attains even larger concentrations. $C_{16}H_8^+$ which is assumed to be a butadiynyl-acenaphthylene ion is also formed at high temperature.

For larger PAH, the number of H atoms depends on the arrangement of rings. Divergence from a more circular system to an elongated or ribbon-like PAH increases the number of hydrogen atoms by 2 or a larger even number, for example



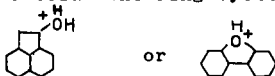
On the other hand



Formation of 5-rings condensed with the 6-rings diminishes the number of H atoms by 2 or a multiple thereof. This possibility of forming relatively hydrogen-poor PAH⁺ is held more probable for high-mass ions.

Of the many possible variations in the number of H atoms for a fixed number of C atoms only a few, seldom more than 3 for odd-numbered and 4 for even-numbered PAH⁺, are realized, even in the case of large PAH⁺. Although there are shifts in the abundance of H-rich and H-poor PAH⁺ with temperature, there is always one certain C-H-composition that dominates in a group of ions with the same number of C atoms. This is always compatible with a highly condensed arrangement of 6-rings with one or no 5-ring. However, in the case of large PAH⁺ these predominant C-H-compositions would also fit to elongated or ribbon-like ring arrangements with an increased number of 5-rings. This option would be in favor of fullerene formation, see below.

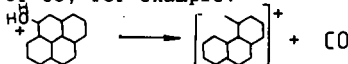
Oxo-PAH⁺, such as C₁₂H₉O⁺, C₁₆H₁₁O⁺ and C₁₈H₁₁O⁺ up to C₃₄H₁₅O⁺, are intermediates in fuel rich benzene flames. They occur together with PAH⁺ [5]. Probably, the positive charge is located on an O atom outside the ring system, for example:



This structure is more stable than



Oxo-PAH⁺ are thermally less stable than PAH⁺ with the same number of C atoms. A primary decomposition step of oxo-PAH⁺ probably is the elimination of CO, for example:



This mechanism of PAH⁺ formation is not taking place in acetylene flames, since no oxo-PAH⁺ are formed from this fuel. Many PAH⁺ in benzene flames contain two more H atoms and probably have structures different from those with the same number of C atoms in acetylene flames. C₁₂H₉⁺ is missing in benzene flames since there is no easy mechanism by which it could be formed through CO elimination from C₁₄H₉O⁺. High-resolution mass spectrometry will show whether such differences in H content do also occur in larger PAH⁺. This might have to do with the stop of PAH⁺ growth at 900 to 1000 u and the absence of charged soot particles in benzene flames up to a C/O = 0.93.

Oxo-PAH⁻ which are only formed in flames of aromatic fuel also decompose within the oxidation zone by elimination of CO giving PAH⁻, for example:



The resulting PAH⁻ with their comparatively stable cyclopentadienyl anion structure, also unique in benzene flames, do not show further growth. That the negative charge of oxo-PAH⁻ is located on the O atom is supported by the fact, that they are able to grow by condensation reactions with lower unsaturated hydrocarbons.

3. POSITIVELY CHARGED SOOT PARTICLES

PAH⁺ with $m \geq 350$ u grow continuously until their average mass reaches about 800 to 1400 u in sooting acetylene flames. Then a new broad distribution of masses ranging from about 2.5 to $7 \cdot 10^3$ u appears. It has a flat maximum at about $4 \cdot 10^3$ u (Fig. 3, 11mm). This is due to the first charged soot particles. About 0.3 ms later (12 mm), it has increased in intensity, peaks at $5 \cdot 10^3$ u and extends to 10^4 u. Meanwhile, the large PAH⁺ have disappeared to a large degree. Instead of a continuous shift of the PAH⁺ distribution into the range of the beginning charged soot, there remains a minimum at about $2 \cdot 10^3$ u. This behaviour is interpreted as a switch from a mainly two-dimensional growth of the PAH⁺ to a three-dimensional growth of soot particles, initiated by sticky collisions of large PAH⁺ with neutral PAH of the same mass range. The total ion concentration stays almost constant between 11 and 12 mm [1].

From 14 mm on, the number density of charged soot particles increases strongly because of the onset of thermal ionization. The further development of the particle mass distributions is shown on Fig. 4, obtained from measurements using a combination Wien-filter/energy discriminator for mass analysis [6].

At the start of soot formation in acetylene flames, the fraction of positively charged soot is very low, of the order of 1%. It increases to 30 - 40% (depending on the burning conditions) when the single particles have reached their final size [7]. Thus, the largest part of positively charged soot is formed by thermal ionization from neutral soot and not as a consequence of growth of PAH⁺. Most of the charged particles carry a single charge. With increasing flame temperature the fraction of doubly charged particles increases up to about 10%. There is also negatively charged soot. It is formed somewhat later and its amount does not reach that of the positively charged soot (15 to 25%). The percentage decreases with increasing flame temperature. As pointed out, PAH⁻ do not grow. Therefore, there is no connection between PAH⁻ and the first negatively charged soot which most probably is formed by electron attachment to neutral particles.

In benzene flames (for C/O < 0.93) the growth of PAH⁺ stops at about $1 \cdot 10^3$ u and only neutral soot is formed thereafter. The reason for this behavior of PAH⁺ is not quite clear. The lower concentration of acetylene and polyynes, the higher temperature together with the partly different structure of PAH⁺ in benzene flames might be the reason. The lack of thermal ionization of soot is caused by the smallness and the slow growth of the first particles in low-pressure benzene flames which is also correlated with the lower concentration of highly unsaturated aliphatics.

4. FULLERENE IONS

Fullerene ions of both sign cover a much larger mass range than PAH ions. The smallest positive ion detected in benzene flames is C₃₂⁺ (384 u). The largest one in sooting acetylene flames exceeds C₅₀₀⁺ (6000 u) as shown by the mass spectrum in Fig. 5. Generally, there are a few outstanding peaks (C₅₀, C₆₀, C₇₀, C₇₄, C₈₂, C₈₄) and a much larger number of quasi-continuously distributed species [5]. A mass spectrum of negative fullerene ions from

the burned gas of a benzene flame in Fig. 6 shows the same general appearance. It differs, however, in some details such as the formation of very small fullerenes like C_{34}^- (smallest in acetylene flames is C_{44}^-) and the occurrence of odd-numbered fullerenes containing 1 to 2 H atoms centered around C_{50}^- and (to a less degree) around C_{70}^- . There are further differences in the ion abundances depending on the height in the flame, the sign and the burning conditions.

The largest difference in the nature of fullerene ions is caused by the onset of soot formation. Fig. 7a demonstrates the change in the fullerene mass spectrum from the soot-free oxidation zone to the soot forming zone in the burned gas of the same benzene flame. A principally similar result was obtained with mass spectra from the burned gas of acetylene flames below and above the critical C/O for soot formation, see Fig. 7b. In both cases the overall abundance of the ions increases and the quasi-continuous distribution of the heavier fullerenes appears when soot is formed. There are mainly some of the outstanding peaks where the fuel-rich flames are free of soot.

In acetylene flames, where the oxidation and the soot-forming zone is clearly separated, the concentration of fullerenes drops to very low values where the temperature is near its maximum and the O_2 is not yet completely consumed. This minimum is specially marked for negative fullerene ions. It is interpreted as burning of the lower-mass fullerenes. A decrease in the total negative ion concentration may contribute to this effect [1]. In benzene flames where these two zones overlap the intermediary decrease is weak for negative fullerenes and not expressed in the positive ion profiles. Formation of fullerenes in the oxidation zone can be suppressed by increasing the temperature.

In the secondary reaction zone of the flame, where O_2 is not yet completely consumed, large fullerene ions of vastly different mass are formed almost simultaneously in the presence of soot. The profiles do not indicate a growth of fullerenes. They reach a second maximum in the burned gas and also decrease simultaneously, probably by charge recombination. The formation of the "prominent" fullerene ions (C_{50} , C_{60} , C_{70}) in this zone is more or less retarded, depending on the burning conditions. In particular, C_{60}^- increases steadily in the burned gas where large negative fullerenes decrease.

While the formation of large PAH may in principle be explained by the growth of lower mass species through reaction with unsaturated C_2 -, C_3 - and C_4 -hydrocarbons and/or the respective radicals, this is not so for the fullerenes. C_{60}^+ is always the first to be observed without being preceded by lower-mass fullerenes. It lies between the C_{50} - and C_{59} -PAH⁺ in the mass spectrum. But these species contain between 18 and 20 H atoms and therefore have quite a different structure. The question is, how might closed-cage molecules (or ions) with 12 five-membered rings be formed in a homogeneous reaction without going through intermediates with too much ring tension.

If the mass spectrum of PAH⁺ is searched for possible "pieces" of C_{60}^+ , the free valencies of which being saturated by H, there are mainly smaller mass PAH⁺ up to 250 u, the C skeletons of which are structural elements of C_{60} . Mass 250 ($C_{20}H_{10}$) could represent a PAH consisting of five 6-rings surrounding one 5-ring. $C_{30}H_{12,13}$ with mass 372 and 373 u which would be the molecular formula for one

"half" of a C_{60} occurs only in very minor concentration. A formation of C_{60} by reactive collision of two half-shells would be too slow because of the low concentrations of the reactants. There is an ion with composition $C_{30}H_6^+$ in very low abundance, which does not fit any C_{60}^+ fragment. The fact that large PAH⁺ with very low hydrogen content could not be detected, indicates that the loss of hydrogen and the formation of most of the 5-rings takes place simultaneously in late stages before completion of the ball. A possible mechanism along these lines might be the following: If two 6-rings at the poles of C_{60} are removed, there remains a closed ribbon of 48 C atoms that unwrapped has the structure



This would correspond to $C_{48}H_{18}$ which is the main C_{48} -PAH⁺. It contains the structural elements of acenaphthylene and benzo[ghi]perylene which are quite common among the PAH. As the number of 5-membered rings is relatively low for the size of the ring system and they are condensed only with four 6-rings, there is no serious ring tension. The molecule bends almost by itself towards closing of the ribbon, see Fig. 8. Most of the C_{48} -PAH⁺ will have flat structures given in section 2, but a few percent might be ribbon-shaped. Addition of two benzene molecules and a rapid stepwise formation of C-C bonds by an intramolecular condensation with simultaneous splitting off of H_2 , while double bonds are regenerated, could finally give C_{60} . This accumulates because of its chemical inertness. The fact that fullerene concentration may be up to ten times larger in benzene flames than in acetylene flames might be an indication that reactions with benzene are important steps. A similar mechanism could be possible for C_{70} . However, there is still no indication how the large fullerenes could be formed, other than probably by heterogeneous reaction which involves very small soot particles.

The authors thank the Deutsche Forschungsgemeinschaft and the Fonds der Chemischen Industrie for financial support.

References

- [1] Ph. Gerhardt, K.H. Homann, *Combust.Flame* 81, 289 (1990)
- [2] Ph. Gerhardt, K.H. Homann, *J. Phys. Chem.* 94, 5381 (1990)
- [3] Th. Baum, P. Weilmünster, K. H. Homann, *Ber. Bunsenges. Phys. Chem.* to be published
- [4] K.H. Homann, U.v.Pidoll, *Ber. Bunsenges. Phys. Chem.* 90, 847 (1986)
- [5] S. Löffler, K.H. Homann, 23rd Symp. Internat. on Combust., The Combustion Institute, Pittsburgh, 1991, in press
- [6] K. H. Homann, J. Traube, *Ber. Bunsenges. Phys. Chem.* 91, 828 (1987)
- [7] K. H. Homann, H. Wolf, 21st Symp. Internat. on Combust., p. 1013, The Combustion Institute, Pittsburgh 1986

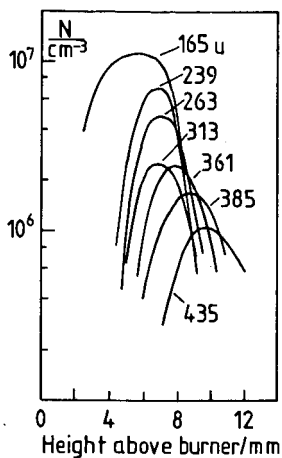


Fig. 1 PAH⁺ profiles in a sooting C₂H₂/O₂ flame; C/O = 1.12; p = 26.6 mbar
v_u = 42 cm/s

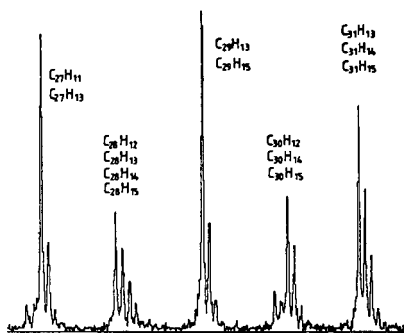


Fig. 2 PAH⁺ with the same number of C occur with different numbers of H; C₂H₂/O₂ = 1.0; p = 26.6 mbar
v_u = 42 cm/s; h = 12 mm

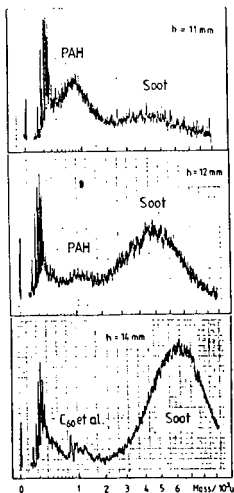


Fig. 3 Mass distributions at the transition from PAH⁺ to charged soot particles; C₂H₂/O₂ = 1.12
p = 26.6 mbar; v_u = 42 cm/s

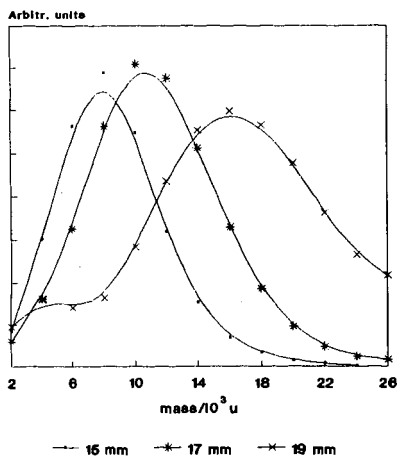


Fig. 4 Mass distribution of charged soot particles in a C₂H₂/O₂ flame; C/O = 1.06; p = 26.6 mbar;
v_u = 50 cm/s

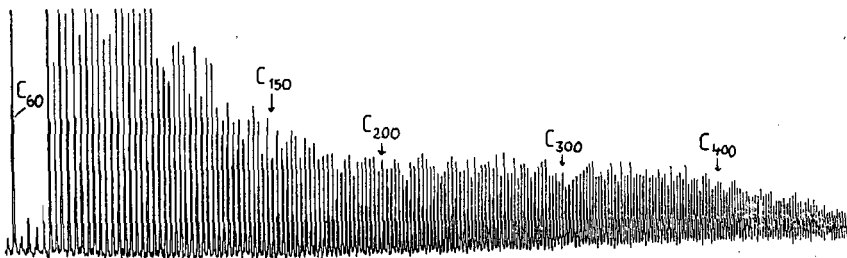


Fig. 5 Mass spectrum of positive fullerene ions from a sooting C_2H_2/O_2 flame; $C/O = 1.0$, $h = 20$ mm, $p = 26.6$ mbar, $v_u = 42$ cm/s. The peaks to C_{104} are truncated.

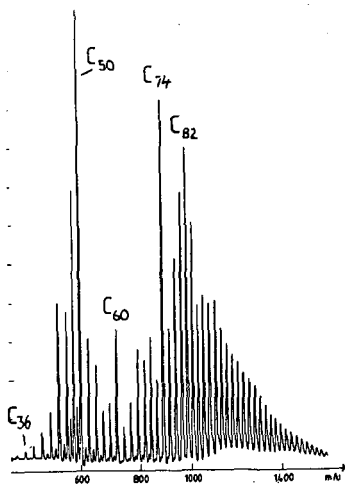


Fig. 6 Mass spectrum of negative fullerene ions from a benzene/oxygen flame; $C/O = 0.76$, $h = 12$ mm, $p = 26.6$ mbar, $v_u = 42$ cm/s

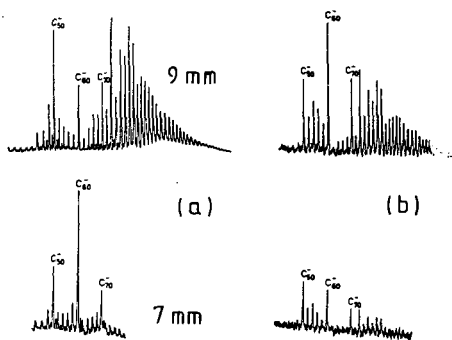
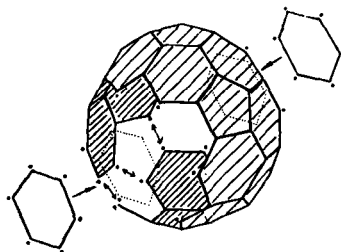


Fig. 7a Negative fullerene ions in the soot-free oxidation zone (7 mm) and in the sooting zone (9 mm) of a C_6H_6/O_2 flame; $C/O = 0.76$, $v_u = 42$ cm/s; 7b: The same ions in the burned gas of a non-sooting (below, $C/O = 0.84$) and a sooting ($C/O = 0.90$) acetylene/ O_2 flame; $h = 28$ mm, $v_u = 42$ cm/s

Fig. 8 Tentative mechanism of C_{60} formation from a bent ribbon-shaped PAH $C_{48}H_{18}$ and two benzene molecules. The dots mark C atoms which carry H atoms while the hidden ones are not marked.



FILUXES AND NET REACTION RATES OF
FLAME SPECIES PERTINENT TO FULLERENES

Christopher J. Pope and Jack B. Howard
Department of Chemical Engineering
Massachusetts Institute of Technology
Cambridge, MA 02139

Keywords: fullerenes, C₆₀, flames

ABSTRACT

Signal intensities of 200+ amu material previously obtained by molecular beam mass spectrometric (MEMS) probing of a low-pressure premixed near-sooting benzene-oxygen flame were analyzed so as to determine mole fractions, fluxes and net reaction rates for 50-amu fractions of high molecular weight flame species. The results show trends indicative of preferential accumulation of mass in the 700-750 amu fraction. The pertinence of these results to Buckminsterfullerene (C₆₀) will be considered, and the observed concentrations will be compared with literature values for C₆₀ ions in similar flames. Mechanistic implication of the presence of fullerenes in a non-sooting flame will be discussed.

INTRODUCTION

Understanding the behavior of molecular weight growth products in flames in the mass range of roughly 300 to 2000 amu has been limited by the scarcity of data for these species. The concentration profiles of chemical species in flames have been measured for compounds as large as C₁₆H₁₀ (MW=202) by molecular beam/mass spectroscopic (MEMS) sampling¹, and C₂₄H₁₂ (MW=300) by gas chromatography (GC)². Homann and coworkers, using MEMS with time-of-flight (TOF) mass spectrometry, have observed in the above mass range both positively- and negatively-charged ions, suspected to be fullerenes^{3,4} and their precursors⁵.

Bittner's MEMS data for a near-sooting (equivalence ratio $\phi=1.8$) benzene-oxygen-30% argon 20-torr flat flame also include high-mass signal profiles for all species with masses greater than a given cutoff value; this cutoff mass was incremented by 50 amu in the range of 200 to 750 amu, inclusive. Howard and Bittner⁶ analyzed these high mass data for the near-sooting flame and similar data from a sooting ($\phi=2.0$) benzene flame, reaching tentative conclusions about the formation and destruction of the high molecular weight material (HMWM) and about its possible role in soot formation. Their analysis of the near-sooting data also gave evidence of the development of a bimodal distribution of the masses of the HMWM with increasing height above burner (HAB). The earlier work was done without detailed flux and rate information, which was later generated by Pope⁷, and with only an approximate treatment of the diffusion of the HMWM.

In the present work, the high-mass signals of Bittner's near-sooting flame are analysed. The earlier analysis of these data by

Howard and Bittner is extended by treating each 50-amu interval as an individual species and by calculating fluxes and net reaction rates for each interval. Approaches used to overcome limitations of the earlier work are discussed. Preliminary analysis of the results gives information on the prevalence and behavior of soot precursors. The results also give evidence consistent with the existence of C_{60} in a non-sooting flame.

TRANSPORT PROPERTIES OF HIGH MOLECULAR-WEIGHT MATERIAL

In flat flames, knowledge of the transport properties of the individual species is essential in obtaining kinetic information from concentration data. Flat flames can be described as one-dimensional plug flow reactors with strong axial diffusion. Due to strong diffusional effects, concentration profiles reflect both transport processes and chemical reaction. Kinetics or rate information is obtained from individual species concentration data by application of the one-dimensional flame equations of Fristrom and Westernberg⁸. The concentration data (as a function of location) are combined with the diffusion equation to obtain molar fluxes of each species at each location; the derivative of the molar flux with respect to distance yields the net reaction rate of the individual species.

The mixture diffusion coefficients used in the calculation are obtained from the binary diffusion coefficients using the relation of Wilke⁹; binary diffusion coefficients are calculated from the Lennard-Jones (12,6) potential. Since the mixture diffusion coefficients depend on the composition of the mixture, and since the composition changes dramatically in the region of interest, the calculation requires concentration data for all flame species.

Treatment of the diffusion of the HMWM required Lennard-Jones parameters. Details of the approach will be published. The correlations of Bird, Stewart, and Lightfoot¹⁰ for the Lennard-Jones parameters as a function of critical temperature (T_c) and critical pressure (P_c) were used. The technique of Forman and Thodos¹¹ for estimating critical properties from molecular structures of hydrocarbons gave values of T_c and P_c . From available data on the molecular structures of flame species observed at the low end of the range of the HMWM, reasonable assumptions were made concerning the molecular structures of expected constituents of the HMWM. The HMWM was assumed to consist of polycyclic aromatic hydrocarbons in the most peri-condensed structures possible for a given carbon number. Peri-condensed PAH structures are the most closely packed arrangement of aromatic rings. For the series of most peri-condensed molecules having only six-membered rings, Lennard-Jones parameters were estimated, and correlated with the molecular weight. Values of the correlated Lennard-Jones parameters for the midpoints of the 50-amu ranges considered (e.g., at 375 amu for the 350-400 amu range) were taken as the Lennard-Jones parameters for that 50-amu range, each range being treated as an individual flame species in the flux and net reaction rate calculations. In the course of the work, Lennard-Jones parameters for fullerenes, and hence species containing both five- and six-membered rings, were also estimated. It was found that replacing the

above calculated transport parameters for the 700-750 amu range with those predicted for C_{60} resulted in only slight quantitative and no qualitative changes in the results.

FLUX AND RATE CALCULATION RESULTS

Mole fraction profiles for selected mass ranges are shown in Figure 1. The profiles exhibit behavior consistent with that of a chemical intermediate; they are first created then destroyed. However, the material heavier than 350 amu is not completely destroyed in the flame being studied. The calculated net reaction rates (Figure 2) also reflect behavior typical of intermediate species, the profiles for each 50-amu fraction having a region of net production followed by one of net consumption. (The wiggles at the extremes of the rate profiles are artifacts of the numerical smoothing and differentiation techniques¹².)

BEHAVIOR OF 700-750 AMU MATERIAL

The results for the 700-750 amu material are different from all the other HMM profiles. The peak of the mole fraction profile is much broader and occurs much farther downstream than is the case for any of the other HMM ranges. The peak value of the mole fraction is also larger than what would be expected from the observed trend of decreasing peak value with increasing molecular weight. The same observations also hold for the molar flux profiles. These results are also reflected in the net reaction rates calculated for the 700-750 amu material. The net production region is wider than that for any of the other 50-amu fractions and the peak is broader. The ratio of the peak destruction rate to the peak production rate is also lower for the 700-750 amu material than for the other HMM.

The results for the 700-750 amu material show that there is a larger amount of material than expected in this molecular weight range, that it is produced over a larger region of the flame, and that it is destroyed more slowly, leading to an accumulation of mass in this size range. The results cannot be explained as the result of PAH coagulation, or in terms of especially stable PAH, but could be explained in terms of an especially stable species which would take longer to form and be more stable than the other PAH species.

The results are consistent with the presence of C_{60} in the near-sooting flame. The stability of C_{60} against attack by radicals has been observed¹³, and in general, the relative abundance of C_{60} compared to other carbon clusters is increased under more severe reaction conditions. Due to its stability, C_{60} is likely to be destroyed more slowly than the HMM, consistent with the accumulation of mass in the 700-750 range. The special structure of C_{60} would likely require more time to be formed than would a flat PAH molecule of comparable size, consistent with the delayed peaks in the 700-750 amu profiles.

COMPARISON WITH OTHER OBSERVATIONS OF C_{60}

Comparison of these results with those of Homann *et al.*³⁻⁵ will be published. Briefly, both studies employed the same type of benzene

flames at the same pressure, but the species measured and the equivalence ratio (ϕ) used in the two cases are different. Therefore the comparison is somewhat complicated and requires explanation. The number concentration profile of 700-750 amu HMWM at $\phi=1.8$ from the present study is compared with the number concentrations of C_{60}^+ at $\phi=1.9$ and C_{60}^- at $\phi=2.15$ found by Homann *et al.*³⁻⁵. The HMWM as measured by Bittner¹ does not include ions. The ions of each species, including C_{60} , are expected to be in much lower concentration than the neutrals. Also, the 700-750 amu HMWM would be expected to include other species in addition to mass 720. For these reasons, the C_{60}^+ and C_{60}^- concentrations should be considerably less than that of the 700-750 amu HMWM. On the other hand, the lower ϕ of the HMWM measurement would be expected to give considerably lower concentrations than would be observed at the higher ϕ 's of the ion measurements. Considering these opposing effects, the two sets of data are found to compare favorably, with no obvious inconsistencies.

REFERENCES

- (1) Bittner, J.D. A Molecular-Beam Mass Spectromete Study of Fuel-Rich and Sooting Benzene-Oxygen Flames; Sc.D. thesis, Department of Chemical Engineering, Massachusetts Institute of Technology, 1981.
- (2) Bockhorn, H.; Fetting, F.; Wenz, H.W. Ber. Bunsenges. Phys. Chem. 1983, **87**, 1067.
- (3) Gerhardt, Ph.; Loffler, S.; Homann, K.H. Chemical Physics Letters 1987, **137**, 306.
- (4) Gerhardt, Ph.; Loffler, S.; Homann, K.H. Twenty-Second Symposium (International) on Combustion, The Combustion Institute, 1988.
- (5) Loffler, S.; Homann, K.H. Twenty-Third Symposium (International) on Combustion, The Combustion Institute, 1990.
- (6) Howard, J.B.; Bittner, J.D. Soot in Combustion Systems and its Toxic Properties, eds. J. Lahaye and G. Prado; Plenum: New York, 1983.
- (7) Pope, C.J. Fluxes and Net Reaction Rates of High Molecular Weight Material in a Near-Sooting Benzene-Oxygen Flame; M.S. thesis, Department of Chemical Engineering, Massachusetts Institute of Technology, 1988.
- (8) Fristram, R.M.; Westenberg, A.A. Flame Structure; McGraw-Hill: New York, 1965.
- (9) Wilke, C.R. Chemical Engineering Progress 1950, **46**, 95.
- (10) Bird, R.B.; Stewart, W.E.; Lightfoot, E.N. Transport Phenomena; Wiley: New York, 1960.
- (11) As discussed in Reid, R.C.; Sherwood, T.K. The Properties of

Gases and Liquids, 2nd ed.; McGraw-Hill: New York, 1966.

(12) Savitsky, A.; Golay, M.J.E. Analytical Chemistry 1964, **36**, 1627. See also corrections by Steinier, et al., Analytical Chemistry 1972, **44**, 1906.

(13) Zhang, Q.L. et al. Journal of Physical Chemistry 1986, **90**, 525.

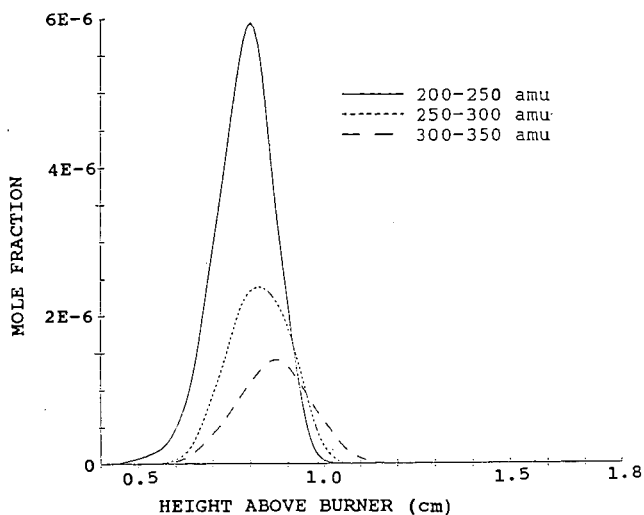


Figure 1: Mole fraction profiles, 200-350 amu.

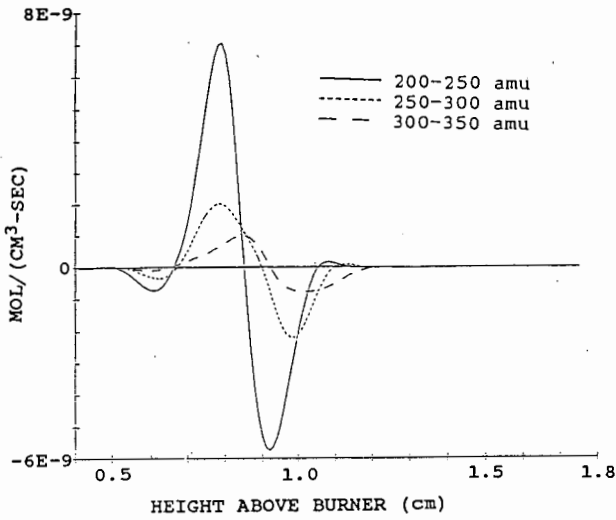


Figure 2: Net reaction rate profiles, 200-350 amu.

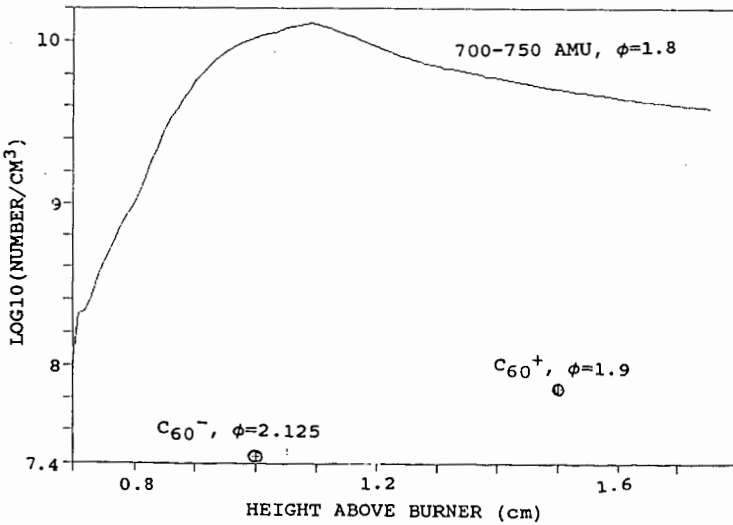


Figure 3: 700-750 mole fraction vs. Homann C_{60} ion measurements

A SHOCK TUBE INVESTIGATION OF SOOT FORMATION FROM TOLUENE/METHANOL MIXTURES. Alexiou, A. and Williams, A., Department of Fuel and Energy, Leeds University, Leeds, LS2 9JT, UK, and Abdalla, A.Y., Helwan University, Cairo, Egypt.

ABSTRACT

Soot formation in toluene and toluene/methanol/argon mixtures was studied behind reflected shock waves using a laser beam attenuation technique. The experiments were undertaken over the temperature range 1484 - 2232K, pressure range 1.69 - 2.77 bar and total carbon atom concentrations for the toluene alone in the range 2.7×10^{17} - 1.1×10^{18} atoms/cm³ (0.5 to 1.5 mol %) and for toluene/methanol mixtures in the range 23 - 66 mol % methanol.

The results indicate that the soot yield decreases with an increase in methanol concentration but the effect is not marked until the addition is greater than 50% methanol. The rates of soot formation from toluene and toluene/methanol mixtures have been determined and exhibit an Arrhenius dependence which was expressed by a correlation equation. The induction periods for soot formation were measured and were found to increase with methanol addition although the maximum soot yields were found to decrease.

INTRODUCTION

Methanol is of considerable practical significance as an alternative fuel or as a blend with petroleum for internal combustion engines. Earlier studies have shown that methanol produces much less soot than typical hydrocarbon fuels but the addition of aromatics greatly increases soot formation (1,2). In contrast, in diesel engines, blends of diesel fuel oil with methanol produce substantially smaller amounts of soot. Surprisingly there has been little previous work on the gas phase combustion of these mixtures and only the benzene-methanol system has been studied by shock-tube techniques (1). In diffusion flames the decreasing fuel type is given by Glassman (3): aromatics > acetylene > olefins > paraffins > alcohols. Since there is usually agreement in the behaviour in diffusion flames and in shock tubes concerning soot tendency, we undertook a shock tube study to evaluate the soot suppression effect. We confined our work to toluene and toluene/methanol mixtures and we present in this paper data on the soot suppression effect of methanol added to toluene mixtures, rather than the alternative approach of adding aromatic fuels to enhance the radiation from methanol flames.

EXPERIMENTAL

The experiments were performed in reflected shock waves and details of the shock tube facility have been previously published (4). The test gas mixtures were prepared manometrically, ANALAR toluene and methanol were further purified by repeated freezing and evacuation. The experimental conditions are summarised in Table 1.

A laser technique was employed and the absorption of the beam at 632.8 nm was used to measure the concentration of soot. Only toluene concentrations up to 1.5 mol % could be studied because of the high levels of absorption. The soot yields were calculated according to Graham's model (5).

$$Y = \frac{C_{\text{soot}}}{C_{\text{total}}} = \left[N \rho \lambda / 72 \cdot \pi \cdot E_{(m)} \cdot \lambda \cdot C_{\text{total}} \right] 2n \left[I_{(o)} / I_{(t)} \right] \quad (1)$$

where C_{soot} = concentration of the particulate carbon per unit volume, C_{total} = the total concentration of carbon atoms per unit volume, N = Avogadro's number, ρ = density of soot, λ = wavelength of the measurement, I = intensity of radiation which is function of time, t , $E_{(m)}^-$ = imaginary part of the function $(m^2-1)/(m^2+2)$, m = the complex refractive index.

Since the soot yield is a function of the refractive index an accurate value is necessary. Many workers, including our previous work, have used the value of Lee and Tien (6) which at this wavelength would give a value of $E_{(m)}^- = 0.174$. In the present work we used the value of $E_{(m)}^- = 0.253$ based on the in flame measurements of Charalampopoulos and Chaung (7). If we had used the Lee and Tien data we would have overestimated the total soot yield as previously observed by Frenklach et al (10); indeed if data by some of the earlier researchers had been used the position would have been worse.

EXPERIMENTAL RESULTS

The results obtained in the toluene pyrolysis experiments are shown in Fig. 1. The amount of soot yield increased monotonically with the amount of toluene pyrolysed. The maximum slope on the oscillogram was measured and defined as the apparent rate of soot formation. The correlation equation of apparent rate of toluene pyrolysis is shown in Fig. 2 for the different concentrations which are given in Table 1. The RH on this figure stands for the fuel concentration term, in this case toluene. The rates exhibited an Arrhenius dependence given by a correlation equation:

$$R_{\text{soot}} \text{ (mol/m}^3\text{s)} = 1.38 \cdot 10^8 [C_7H_8]^{1.32} \exp(-11,900/T) \quad (2)$$

The activation energy which is valid up to 1950 K (1532 - 1950 K) is in agreement with the values quoted by Simmons and Williams (9), namely 99 - 118 kJ/mol depending on the value of the refractive index. The constant and the fuel exponent have changed because of the improved accuracy of the present data. The fuel exponent is now consistent with the value of 1.48 reported by Wang et al (8).

During the course of toluene/methanol pyrolysis mixtures an induction time was observed before any absorption occurred. This induction time was the time between the reflected shock wave and the onset of soot formation. Figure 3 shows the results for the induction times. As it can be seen the induction time increased with the amount of methanol added to the toluene. The following equation for calculating the soot induction time, t_{soot} , based on a 5% rise in signal was obtained.

$$t_{\text{soot}} = 5.448 \cdot 10^{-5} [\text{total fuel}]^{1.92} \exp(-16,644/T) \quad (3)$$

where [total fuel] = $[C_7H_8 + CH_3OH]$. The soot yield decreased monotonically with the increase of the amount of methanol added to toluene as shown in Fig. 4.

The apparent rate of toluene/methanol pyrolysis are measured in the same way as toluene and could be expressed as follows:

$$R_{\text{soot}} \text{ (mol/m}^3\text{s)} = 1.9 \cdot 10^5 [\text{total fuel}]^{-0.412} \exp(-15,300/T) \quad (4)$$

which is valid in a temperature range 1580 - 1950 K.

Fig. 5 shows the correlation equation of the apparent rate of soot formation of toluene methanol mixtures at different concentrations (Table 1).

We attempted to obtain a correlation equation incorporating both $[C_7H_8]$ and $[CH_3OH]$ terms, but we had great difficulty in separating the terms in an equation

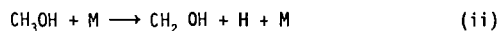
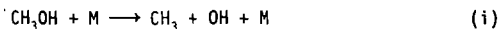
of, for example, the form $R_{\text{soot}} = C_1 [C_7H_8]^a \exp(-E_1/RT) - C_2 [CH_3OH]^b \exp(-E_2/RT)$. Even though the correlation which we obtained is not ideal it can be used to express the rates and by comparing equations (2) and (4) conclusions could be made about the role of added methanol. The experimental determined exponent of the fuel term indicates that an increase of methanol concentration will decrease the apparent rate of soot formation. In addition there are differences in the activation energies and in the pre-exponential factor which are very significant.

DISCUSSION

In the early work by Graham (5) the extent of conversion of initial carbon in the fuel to soot was determined at 2.5 ms. Based on this observation time the soot yield fell rapidly with increasing temperature from 100% at ≈ 1800 K to less than 5% at 2300 K. He developed his well-known scheme which involved condensation reactions at around 1000 to 1800 K and fragmentation reaction above that temperature. Later Frenklach (10) demonstrated that the soot yield is not universal, but is dependent on experimental controllable variables such as observation time, total pressure and laser wave-lengths. He postulated another model for soot formation included polymerisation and fragmentation reactions.

In our work we measure the maximum conversion of the fuel to soot irrespective of the time. As is shown in Fig. 1, the maximum yield occurs at ≈ 1900 K above which fragmentation takes place resulting in a reduction in soot yield. Based on this observation we do agree with Frenklach (10) that the soot yield maximum is not universal and the condensation, fragmentation reactions take place according to experimental conditions.

The unimolecular decomposition of methanol at high temperature is considered to involve two reactions (11).



A computer model for toluene/methanol pyrolysis has been developed in which the initiation reactions (i) and (ii) of methanol together with the low activation energy reactions of H and CH_3 with CH_3OH has been used in order to evaluate the reduction of the soot yield. Preliminary results at about 1900 K not surprisingly demonstrate the importance and the rapid formation of OH and the products H_2O and CO increasingly as methanol is added to toluene. These reactions are also responsible for the increased soot induction period. Therefore it seems that the presence of OH radicals when methanol is added to toluene leads to the behaviour observed experimentally. These results are consistent with the role of OH as an oxidant in carbon-forming flames (12).

More recently, Frenklach (1), in his work on alcohol addition, explained that the reduction is also due to hydrogen atom scavenging. Alcohols undergo the H-abstraction reactions which results in the reduction in the superequilibrium of H atoms. In toluene pyrolysis the overshoot of hydrogen atoms beyond their equilibrium concentration is responsible for the propagation of the ring growth process. Our work is consistent with this since we demonstrate this soot reduction and this effect is not marked until the addition is greater than 50 mol % methanol.

Finally it should be noted that these results are consistent with the behaviour of methanol in fuel blends for gasoline engines. In the case of diesel engines the marked reduction in soot yields cannot arise from gas phase reactions alone and must arise from some physical change such as selective droplet evaporation or disruptive burning.

CONCLUSIONS

The results of the present study show that methanol acts as a suppressing agent for soot formation. However this reduction is only achieved when the presence of methanol exceeds more than 50% in the total fuel mixture to be pyrolysed.

ACKNOWLEDGEMENTS

One of the authors (AA) would like to thank the Esso Petroleum Company Ltd. for financial support and the British Council for support (AYA).

REFERENCES

1. M. Frenklach and J. Yuan. 17th Int. Symp. on Shock Tubes and Waves, 1989, pp 487-493.
2. M. Nakamuza, S. Koda and K. Akita. 19th Symp. Int. on Comb., 1982, pp 1395-1401.
3. I. Glassman. Combustion 2nd Edit. Academic Press, Orlando, Florida, 1987.
4. C.M. Coats and A. Williams. 17th Symp. Int. on Comb., 1979, p 611.
5. S.C. Graham, J.B. Homer, J.L.D. Rosenfeld. Proc. R. Soc. London, A344, 1975, pp 259-285.
6. S.C. Lee and C.L. Tien. 18th Int. Symp. on Comb., 1981, p 1154.
7. T.T. Charalampopoulos and H. Chung. Comb. Scien. and Techn., 1988, vol. 59, pp 401-421.
8. T.S. Wang, R.A. Matula, R.C. Farmer. 18th Symp. Int. on Comb., 1981, pp 1149-1158.
9. B. Simmons and A. Williams. Comb. & Flame, 1988, 71, pp 219-232.
10. M. Frenklach, S. Taki, R.A. Matula. Comb. & Flame, 1983, 49, pp 275-282.
11. P.H. Gribb, J.E. Dove, S. Tamazuki. 20th Int. Symp. on Comb., 1984, pp 779-787.
12. K.G. Neon, J.D. Howard, A.F. Sarofim. Particulate Carbon Formation During Combustion, Plenum press, New York, 1981.

TABLE 1

	% Mol in Argon	T (K)	P (bar)	Carbon (atoms/cm ³)
1	0.5 C ₇ H ₈	1580 - 2170	1.81 - 2.62	2.54 x 10 ¹⁷ - 3.01 x 10 ¹⁷
2	1.0 C ₇ H ₈	1532 - 2114	1.74 - 2.70	5.83 x 10 ¹⁷ - 6.56 x 10 ¹⁷
3	1.5 C ₇ H ₈	1584 - 2070	1.93 - 2.89	9.38 x 10 ¹⁷ - 1.07 x 10 ¹⁸
4	1.0 C ₇ H ₈ + 0.3 CH ₃ OH	1600 - 2096	1.85 - 2.67	6.19 x 10 ¹⁷ - 6.85 x 10 ¹⁷
5	1.0 C ₇ H ₈ + 0.5 CH ₃ OH	1580 - 2123	1.82 - 2.77	6.33 x 10 ¹⁷ - 7.19 x 10 ¹⁷
6	1.0 C ₇ H ₈ + 1.0 CH ₃ OH	1610 - 2087	1.88 - 2.79	6.65 x 10 ¹⁷ - 7.84 x 10 ¹⁷
7	1.0 C ₇ H ₈ + 2.0 CH ₃ OH	1664 - 2050	2.06 - 2.79	8.17 x 10 ¹⁷ - 8.94 x 10 ¹⁷

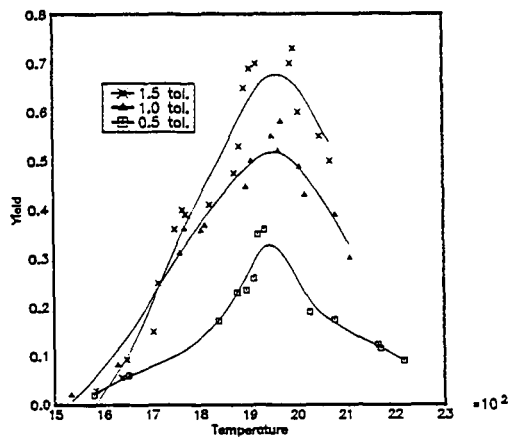


Fig. 1. Comparison of the soot yield at different toluene concentrations.

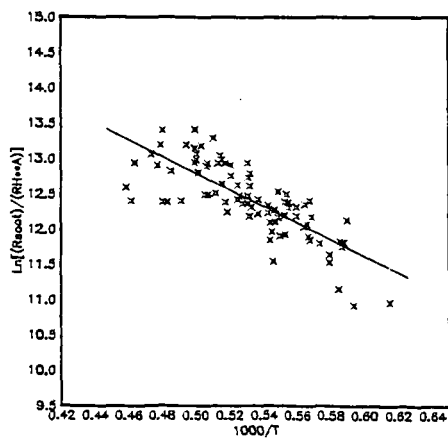


Fig. 2. Correlation equation of apparent rate of soot formation from toluene pyrolysis at different concentrations.

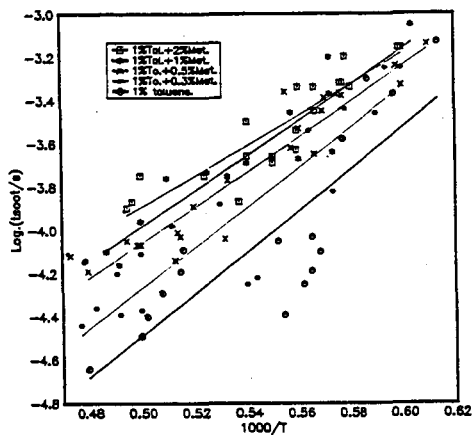


Fig. 3. Induction times for soot appearance at different toluene/methanol concentration.

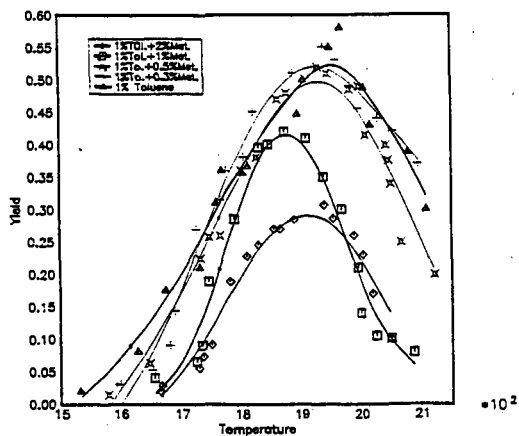


Fig. 4. Comparison of the soot yield at different toluene/methanol concentrations.

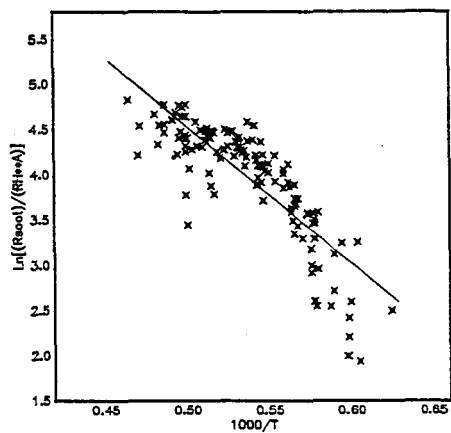


Fig. 5. Correlation equation of apparent rate of soot formation from toluene/methanol pyrolysis at different concentrations.

FORMATION OF VOLATILE PRECURSORS OF NO_x
IN THE RAPID PYROLYSIS OF NITROGEN-CONTAINING HETEROAROMATICS

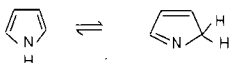
J. C. Mackie and A. Doughty
Department of Physical and Theoretical Chemistry
University of Sydney
NSW 2006, Australia

Keywords: pyrolysis, NO_x precursors, heteroaromatics

INTRODUCTION

Identification of the reaction pathways whereby fuel-bound nitrogen evolves as NO_x in the combustion of low rank fuels has attracted considerable recent attention. As models for the evolution of NO_x from coal combustion, compounds containing the six-membered heteroaromatic pyridine ring and the five-membered pyrrole ring are being investigated. Recently, we have studied the kinetics of pyrolysis of pyridine¹ by single pulse shock tube techniques and developed a detailed kinetic reaction mechanism to model the observed products of decomposition. Pyridine was found to decompose principally via a hydrogen chain mechanism involving abstraction of the ring hydrogen *ortho* to the nitrogen atom, followed by ring scission of the *o*-pyridyl radical to an open-chain radical which could eliminate acetylene and form the HC=CH-CN radical which may eliminate H and form cyanoacetylene or produce acrylonitrile via an abstraction route. HCN was found to be largely a secondary product of pyrolysis of these organic nitriles and also of acetonitrile.

More recently, our investigations of the kinetics of pyrolysis of pyrrole² have shown that the five-membered heterocycle decomposes very differently from the six-membered heteroaromatic. Isomerization followed by ring opening to the open-chain C₃H₃CN isomers of pyrrole predominates the mechanism. Our interpretation of the kinetics has assumed that the decomposition is initiated by the reversible tautomeric reaction



to form the 2-H pyrrole (pyrroline) with subsequent rupture of the weaker C2-N bond in the 2-H tautomer. It has been shown^{2,3} that only through secondary decomposition of the C₃H₃CN products (principally *cis*- and *trans*- crotonitrile and allyl cyanide) are the NO_x precursors including HCN produced. Thus, an understanding of the pathways of NO_x formation from pyrrole rings requires a knowledge of the thermal decomposition kinetics of the C₃H₃CN isomers of pyrrole. This is considered in one part of this paper.

In heavy fuels heteroatoms are often found in condensed ring environments and in substituted rings rather than in the simple unsubstituted five- and six-membered rings. Evolution of NO_x precursors might well depend upon the degree of heteroatomic ring substitution or condensation. The present work therefore involves, in part, a study of the simplest ring substituted heteroaromatic, 2-picoline (2-methylpyridine), the heteroaromatic analogue of toluene, whose stabilized radical, benzyl plays an important role in aromatic hydrocarbon pyrolyses and oxidations. Its heteroaromatic radical analogue, 2-picolyl might also be expected to be a key radical in heteroaromatic oxidations.

EXPERIMENTAL

Kinetics of pyrolysis of the nitrogen-containing products (cis- and trans-crotonitrile, allyl cyanide and 2-picoline) have been studied dilute in argon (0.1–0.4 mol%) in a single-pulse shock tube (SPST) over the temperature range 1100 to 1700 K, at pressures from 17–23 atm and at uniform residence times behind the reflected shock front of 600–800 μ s. Analyses of products and remaining reactant have been made by capillary column GC. Product identifications have been made, where possible by comparison of retention times with standard samples, after initial identification by GC/MS and, in some cases, by FTIR spectrometry. The shock tube is equipped with pairs of UV-transmitting sapphire windows adjacent to the endwall. The absorption spectra of 2-picoline vapour and its products of decomposition have been measured over the wavelength range of 250–350 nm at a distance of 35 mm from the endwall with a detection system of time constant ≤ 5 μ s. Details of the shock tube and ancillary analytical system are presented in our earlier publications.^{1,2} Samples of each compound studied were purchased from Aldrich of 98–99% purity and were further purified by several bulb-to-bulb distillations to greater than 99.8% (by GC) in all cases. Pressures and temperatures behind the reflected shock were computed from measurements both of incident and reflected shock velocities.

RESULTS AND DISCUSSION

Secondary Decomposition of Pyrrole Pyrolysis Products

Figures 1(a)–(d) illustrate the temperature profiles of all products of significance for both allyl cyanide and crotonitrile pyrolysis. The same set of products was observed irrespective of whether the initial reactant was allyl cyanide or crotonitrile, with only the relative yields of the products changing with starting isomer. HCN, acetylene, acetonitrile and acrylonitrile were all observed at very low extents of decomposition, and remained the major products at high extents of decomposition. Minor nitrogen-containing products were ethyl cyanide, cyanoacetylene, and cyanopropyne/cyanoallene. Methane was also present in significant concentrations, along with smaller quantities of ethylene, propene and propyne. Traces of the following compounds could also be detected: cis- and trans- 1-cyano(1,3-)butadiene, benzonitrile, pyridine, diacetylene, 1,3-butadiene, 1-butene, benzene and toluene. The major difference in product distributions between the reactants crotonitrile and allyl cyanide was that allyl cyanide yielded significantly higher proportions of HCN, acetonitrile, acetylene and ethylene. C₃ hydrocarbons were also generated in higher concentrations for allyl cyanide when compared with crotonitrile. No dependence of the rate of decomposition of the reactant on initial concentration was observed.

The product distribution observed in the pyrolysis of the butenenitriles can best be described in terms of a free radical mechanism. The observation of a mixture of C₂H₂CN isomers in the product mixture shows that isomerization of the starting isomers occurs simultaneously with decomposition. Although there are considerable uncertainties in the thermochemistry of some of the nitrogen-containing radicals produced, it would appear that the most likely initiation reaction for the free radical mechanism would occur through single C–C bond fission. For crotonitrile, C₃–C₄ bond fission [reaction (1)] would be expected to take place whereas with allyl cyanide C₂–C₃ fission (2) would be most favourable.



Although initiation through C–H bond fission is possible, the significantly higher C–H bond energy

would make this only a minor initiation pathway. Thermochemical parameters for radicals and other species of importance in this study are given in Table 1. In the Table certain of the heats of formation have been obtained from kinetic modeling of pyrolysis kinetics. Entropies and heat capacities have been obtained by approximate Third Law calculations.

Formation of the major products, acetylene and acetonitrile, can be modeled by means of a simple abstraction chain mechanism in which the abstracting radical is CH_2CN . See Figure 2. A major intermediate in this mechanism would appear to be the cyanoallyl radical, $\text{C}_3\text{H}_3\text{CN}$. Analogous with allyl itself, we would expect this radical to possess resonance stability. Fission of a C-C bond in this radical would seem less likely than rearrangement to a less stable radical whose bond fission leads to C_2H_2 and to regeneration of CH_2CN . Both vinyl and its cyano- analogue, cyanovinyl ($\text{HC}=\text{CHCN}$), should readily undergo unimolecular C-H fission, on the one hand to acetylene, on the other, to produce the observed cyanoacetylene. Hydrogen atom addition, either to the double bond of $\text{C}_3\text{H}_3\text{CN}$ or to the nitrile group can produce another set of observed products, including the major products acrylonitrile and HCN. (See Figures 3 and 4). A detailed kinetic model comprising 107 reactions which include both abstractions and H additions as well as isomerization reactions of the $\text{C}_3\text{H}_3\text{CN}$ isomers, has been used to satisfactorily model the major and minor products of the pyrolyses of crotonitrile and allyl cyanide.⁴ Examples of the comparison between model predictions and experiment are given for some major products in Figure 5.

Pyrolysis of 2-picoline

2-Picoline may be considered to be the nitrogen heteroaromatic analogue of toluene. Behind reflected shock waves at residence times of about 800 μs and 20 atm, 2-picoline begins to dissociate at about 1250 K. Principal products of decomposition are HCN and C_2H_2 although cyanoacetylene, acrylonitrile and acetonitrile are significant nitrogen containing products. 2-Ethylpyridine and pyridine, especially at lower temperatures, are also observed. By analogy with toluene, we would expect the pyrolysis to be dominated by reactions of the 2-picoly radical, the analogue of benzyl. Troe et al^{5,6} have made an extensive investigation of the electronic absorption spectra of benzyl and benzyl decomposition fragments in both thermal and laser decomposition of toluene and side-chain substituted derivatives. They found that the spectral region around 300 nm in shock heated toluene is dominated by benzyl radical and benzyl products spectra.

Similarly we find the the absorption spectrum between 300-340 nm of shock heated 2-picoline is dominated by absorbing species which show strikingly similar temporal behaviour to those reported by Troe et al^{5,6}. Figure 6 gives an example of the spectrum of decomposing 2-picoline vapour (0.2%) in argon at a temperature of 1634 K. Note the rapid rise in absorption to an initial steady state, followed by a longer time steady rise in absorption. The absorption is most probably the consequence of at least two absorbers, the first a species which undergoes rapid equilibration followed by slower decomposition to a more stable product or products. Similar observations in toluene decomposition have by attributed by Troe et al^{5,6} to the initial formation of benzyl radicals which equilibrate rapidly owing to an unexpectedly high value of the rate constant for recombination



Slower decomposition was attributed to homogeneous recombination of benzyl radicals to produce dibenzyl which eventually underwent successive H fissions to the highly absorbing molecule, stilbene.

It is therefore tempting in our 2-picoline studies to assign the initial absorber of 330 nm radiation to the 2-picoly radical, which, like benzyl, must also undergo rapid recombination with H atoms. The slower increase in absorption would therefore be associated with 2-picoly reaction products

which are sufficiently conjugated to absorb strongly around 330 nm. It would seem that such chromophores are not very volatile since no absorption around 330 nm can be detected in the absorption spectra of the products when cooled to room temperature.

More work is required to establish that the initial carrier of 330 nm radiation is the 2-picoly radical in the pyrolysis of 2-picoline. If, tentatively, we assume that the pyrolysis of 2-picoline is initiated by H atom fission to form 2-picoly radical (reaction 3) then the value given in Table 1 for the heat of formation of this radical is in accord with our experiments. Values for the entropy and heat capacity of this radical have been obtained by a Third Law calculation in which vibrational frequencies of the radical have been estimated from those of toluene, benzyl and 2-picoline^{5,7} and moments of inertia calculated from an estimated geometry.

ACKNOWLEDGEMENTS

Mr A. Terentis is thanked for assistance with the experiments on 2-picoline.

REFERENCES

1. Mackie, J.C., Colket, M.B. and Nelson, P.F., *J. Phys. Chem.*, **94**, 4099, (1990).
2. Mackie, J.C., Colket, M.B., Nelson, P.F. and Esler, M., *Int. J. Chem. Kinet.* (in press)
3. Lifshitz, A., Tamburu, C. and Suslensky, A., *J. Phys. Chem.*, **93**, 5802, (1989).
4. Doughty, A., B.Sc.(Hons.) Thesis, University of Sydney, 1990, Doughty, A. and Mackie, J.C. (to be published)
5. Muller-Markgraf, W. and Troe, J., *J. Phys. Chem.*, **92**, 4899, 4905, (1988).
6. Hippler, H., Reihs, C. and Troe, J., *Z. Phys. Chem. N.F.* **167**, 1, (1990).
7. Scott, D.W., Hubbard, W.N., Messerly, J.F., Todd, S.S., Hossenlopp, I.A., Good, W.D., Doulin, D.R. and McCullough, J.P., *J. Phys. Chem.*, **67**, 680, (1963).
8. King, K.D. and Goddard, R.D., *J. Phys. Chem.*, **80**, 546, (1976).

Table 1. Thermochemical data for nitrogen-containing compounds

Species	$\Delta H_{f,300}$ kcal/mol	$S_{f,300}$ cal/K /mol	C_p cal/K/mol					Ref.
			300	500	1000	1500	2000	
CH ₂ CN	59.0	59.8	12.3	15.5	20.2	22.6	29.3	8
HC=CHCN	97.9	67.2	15.9	19.8	25.3	27.8	29.3	PW
H ₂ C=CHCHCN (cyanoallyl)	77.0 ^a	73.0	19.1	28.0	39.2	43.6	46.1	PW
HC=CHCH ₂ CN	91.6 ^a	80.3	21.1	28.0	39.2	42.7	45.4	PW
H ₃ CCH=CHCN	85.0 ^a	76.5	22.3	32.1	45.5	51.0	54.4	PW
H ₃ CCH=CHCH=N	80.6	76.5	22.3	32.1	45.5	51.0	54.4	PW
Py ^a	81.7 ^a	72.6	18.0	28.9	42.8	48.5	51.1	1
PyCH ₂ ^b	65 ^a	78.1	25.4	38.9	56.4	63.8	67.5	PW

^aortho-pyridyl radical ^bortho-picoly radical PW: present work

^aValue derived from kinetic modeling.

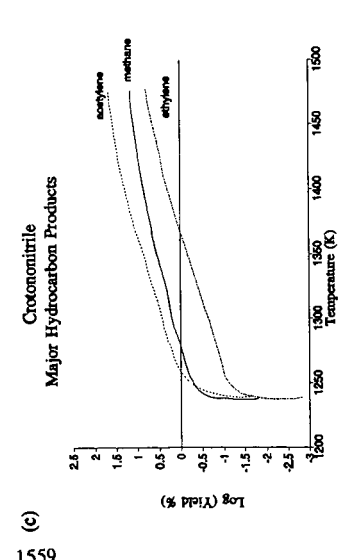
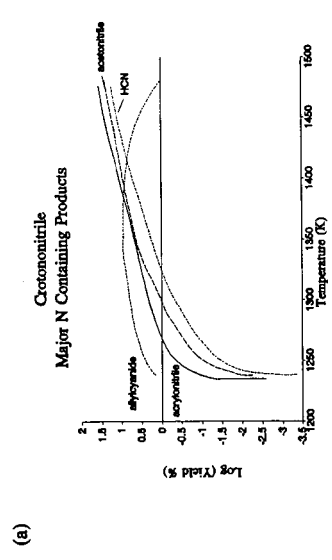
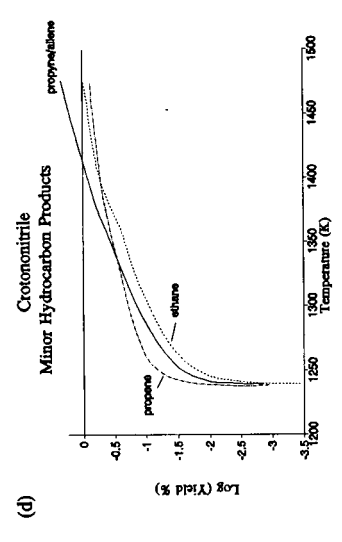
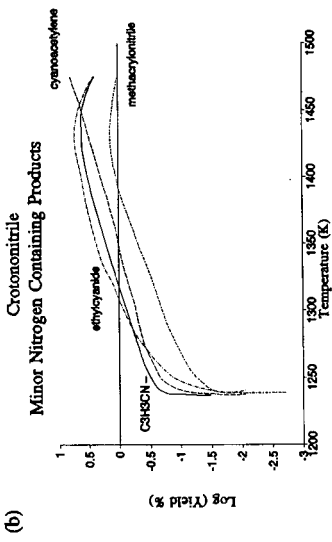


Figure 1. Products of pyrolysis of crotonitrile.

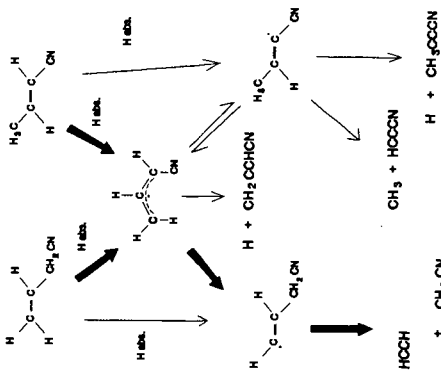


Figure 2. Free radical chain mechanisms.

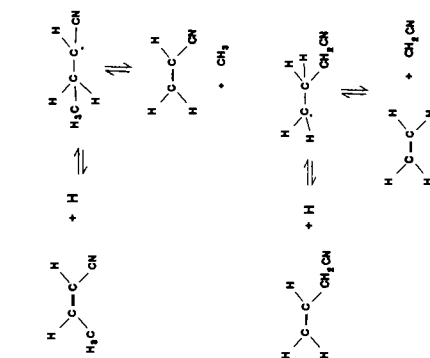


Figure 3. H additions across the double bond

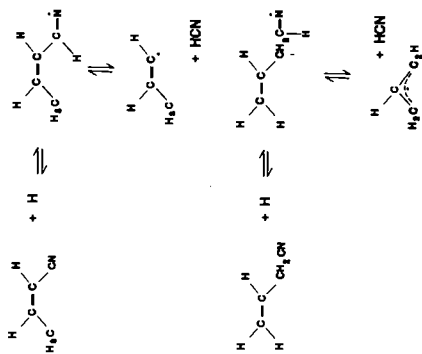


Figure 4. H additions to the nitrile group

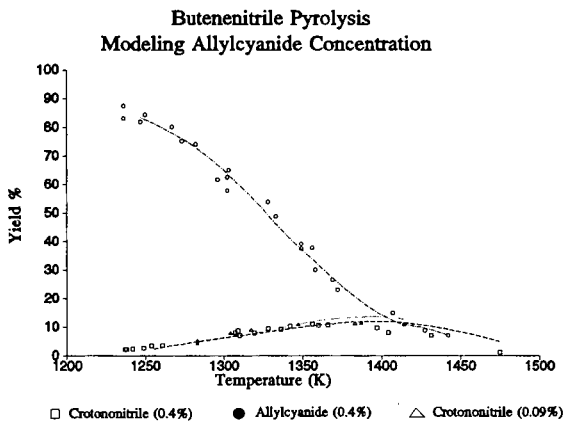


Figure 5(a). Modeling of Allylcyanide Concentration :
(points indicate experimental values , lines model predictions.)

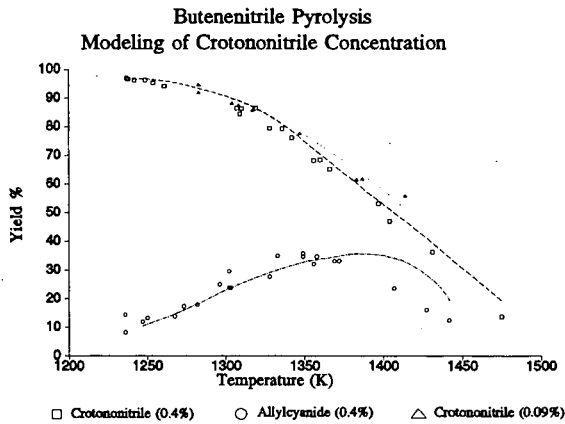


Figure 5(b). Modeling of Crotononitrile Concentration :
(points indicate experimental values , lines model predictions.)

Butenenitrile Pyrolysis
Modeling of HCN Formation

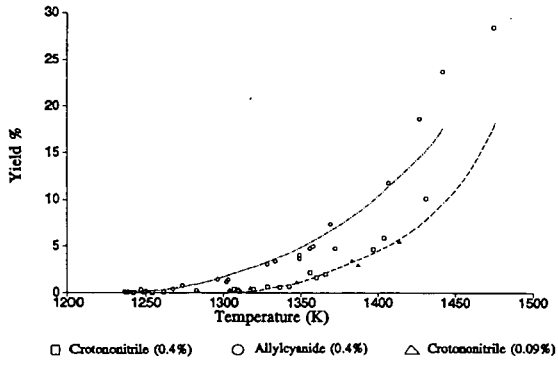


Figure 5(c). Modeling of HCN Formation :
(points indicate experimental values ; lines model predictions.)

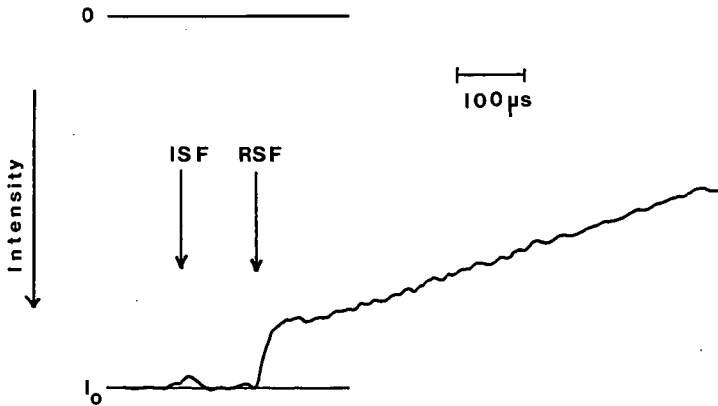


Figure 6. Time dependence of an oscilloscope trace recording the absorption of 330 nm radiation in the pyrolysis of 2-picoline at 1634 K and 20 atm. ISF denotes the arrival of the incident shock front at the observation window, RSF denotes reflected shock front.